Rules and methods for dimensioning embarked materials for surface ships when subjected to UNDEX

Mauricio García Navarro

Master Thesis

presented in partial fulfillment
of the requirements for the double degree:
“Advanced Master in Naval Architecture” conferred by University of Liege
"Master of Sciences in Applied Mechanics, specialization in Hydrodynamics, Energetics and Propulsion” conferred by Ecole Centrale de Nantes

developed at West Pomeranian University of Technology, Szczecin
in the framework of the

Supervisor:	Prof. Hervé Le Sourne, Institut Catholique d'Arts et Métiers (ICAM), Nantes
Reviewer:	Prof. Philippe Rigo, University of Liege

Nantes, February 2015

CONTENTS

DECLARATION OF AUTHORSHIP

I declare that this thesis and the work presented in it are my own and has been generated by me as the result of my own original research.

Where I have consulted the published work of others, this is always clearly attributed.

Where I have quoted from the work of others, the source is always given. With the exception of such quotations, this thesis is entirely my own work.

I have acknowledged all main sources of help.

Where the thesis is based on work done by myself jointly with others, I have made clear exactly what was done by others and what I have contributed myself.

This thesis contains no material that has been submitted previously, in whole or in part, for the award of any other academic degree or diploma.

I cede copyright of the thesis in favour of Institut Catholique d'Arts et Métiers (ICAM), Nantes

Date: 01/19/2016 Signature Mauricio García Navarro

ABSTRACT

This Master thesis is dedicated to the study of the different rules available in order to perform the analysis for surface ship during an underwater explosion (UNDEX). The document performs a review of the up-to date techniques used in order to perform an UNDEX analysis, as well as the different equations and variables which are present during this type of event, exploring the different formulation available.

Since the tools used to perform a ship UNDEX analysis must take into account complex behavior, such as the fluid structure interaction and cavitation effects, formulations which are included in commercial codes are also exposed with some examples. At the same time, some comparisons are showed between numerical simulations obtained using professional codes and simplified formulation. The compare results are plastic strain, and stress levels, as well as displacement time histories obtained at some points of the structure being analyze.

Furthermore the document explores the different rules available for the design of structures subjected to an UNDEX, and points out the common information between all of the documentation available. This information is then used for the construction of a new procedure that will highlight the main consideration in order to perform an UNDEX analysis.

The procedure in then applied to the elastoplastic response analysis of a ship section submitted to a spherical shock wave. Bottom deflection and plastic strains, calculated by two different nonlinear finite element codes, are compared. The first code, used by STX France, is based on an implicit time integration solver, while the second one, used in ICAM, is based on an explicit one.

Finally some conclusions on the obtained results are presented and some recommendations on nonlinear response analysis of naval structures submitted to underwater explosions are given.

1. INTRODUCTION

This Master Thesis counts the different methods to lead the development of tools to the correct design of surface vessels to withstand an explosion located at the sea, such as the ones produced by mines, torpedoes or vessel.

The first works regarding the UNDEX and its effect on the hulls of vessels, has been reported since 1860, and many system were tested before the beginning of the World War I by many countries, and then extensively improved at the arrival of the World War II. The analysis performed at this time was the development of test models replicating the same condition as the one given during the war. These models and the data obtain from the incidents lead to development of better designs, this include the use of different materials, and different structural arrangements.

At the year 1923 the gas bubble effect was discovered, and the effects of the pulsation generated during these physical phenomena were studied. It was the first time that mathematical models were then obtained to describe the large pressures obtained regarding the expansion of the gas bubble, as well as the radius (Keil, 1961). At this point the it was noticed that the oscillations caused by the bubble effect were also dangerous not only because of the large wave shock at the beginning of the explosion, but also because of the effect of the pulsation during the expansion and contraction bubble, that could happen to have the same resonance with the main harmonics from the hull girder structure; causing large deformation to the structures, and eventually the failure of the structure or key components from the vessel.

The response for surface vessels to shocks is now a chapter that is open not only for military vessels, but also for normal vessels concerning accidental scenarios. For instance, the continuous increasing grow of the offshore oil extraction, is one of the activities that have led to the disclosure of this topic, in order to achieve certain safe standards.

Now a days, due to the elements which are available, an due to the effect of the big cost that will demand that will take to develop trials, the simulation has become one of the best tools available to perform a good estimation.

2. UNDERWATER EXPLOSIONS: GENERAL REVIEW RULES AND PROCEDURES

An underwater explosion is defined as one produced by a highly energetic thermochemical reaction inside the water as mentioned by (Reid, 1996) (Mehaute & Wang, 1996).This kind of explosions can produce a high damage to a vessel, if compared to another with similar size at middle air. What makes an underwater explosion dangerous is the fact that, the water becomes the perfect media to transmit the pressure due to its low compressibility. Figure 1 shows the effects of the bubble pulsation, and the general behaviour of the exponential decay pressure of an UNDEX.

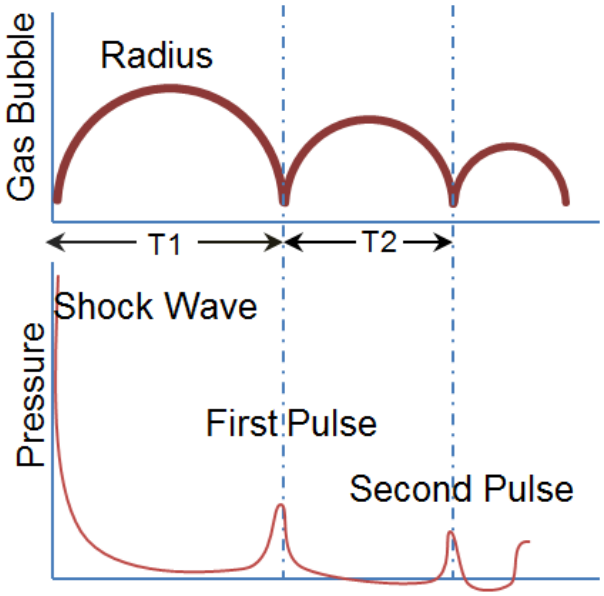

Figure 1. Schematic representation of shockwave pulsation during time. Available from (Keil, 1961).

The exponentially decaying shockwave is propagated, as a spherical wave and which is much faster than the speed of sound (1500 m/s). In general, an underwater explosion is characterized by the formation of a gas bubble which will expand until a point at which hydrostatic pressure will impede its expansion. At this point the flow of the water will begin to go inwards, until again the energy produced by the explosion catches up. This process of expanding and shrinking is characterized by fluctuation of pressure called pulsations. These following wave pressure peaks after the first wave pressure shock, are lower than the initial peak. At the time of the explosion, the bubble also starts to migrate upwards, achieving the largest migration or upward movement when it is found at a contraction phase.

2.1. Parameters that define an UNDEX

The mathematical model for a shockwave described by (Reid, 1996), shows an immediate rise of pressure, followed by an exponential decay. At an initial point, the velocity which is proportional to the peak pressure usually falls down rapidly following an exponential decay, this later depending on the size of the explosive, the size of the charge, and the stand-off distance. As described by (Cole, 1946) the maximum pressure peak obtained by an underwater explosion can be defined by the following equation:

$$P_0 = f\left(\frac{W}{R}\right) \tag{1}$$

Where *W* which is the size of the explosive and R which is the standoff distance at the point being measure. The formulation described by (Reid, 1996) gives the following expression:

$$\mathrm{P_0} = \mathrm{K1}\left(\frac{\mathrm{W}^{1/3}}{\mathrm{R}}\right)^{\mathrm{A1}} \tag{2}$$

The value *Po* is the ***peak pressure*** in MPa, *W* is the weight of TNT in Kilograms, and *R* is the Stand-off distance in meters. The pressure follows an exponential decay defined by the equation:

$$P_m(t) = K1\left(W^{1/3}/R\right)^{A1} \cdot e^{\frac{(t-to)}{\theta}} \tag{3}$$

Where $P_m\,(t)$ is usually defined as the free field pressure. The value of to represents the initial time at which the shockwave arrives at the distance *R*, and *t* is the time elapsed since the shockwave arrived at the distance *R* and θ is the decay time constant, or the equivalent time that it takes for the pressure to decay (1/e).

$$\theta = K2\ W^{1/3}\left(\frac{W^{1/3}}{R}\right)^{A2} \tag{4}$$

The impulse function of the blast can be described as the integral of the pressure along the time lapse of the blast:

$$I(t) = \int_0^t P(t)dt \tag{5}$$

That can also be expressed as:

$$I(t) = K3\ W^{1/3} \left(\frac{W^{1/3}}{R}\right)^{A3} \tag{6}$$

The shockwave energy can be defined as the work done over a surface, or the energy available per unit of area. It can be expressed using the following equation.

$$E(t) = \frac{1}{\rho c}\int_0^t P(t)^2 dt \tag{7}$$

In the same way:

$$E(t) = K4\ W^{1/3} \left(\frac{W^{1/3}}{R}\right)^{A4} \tag{8}$$

The maximum radius of the bubble can be obtained by:

$$R_{max} = K5 \left(\frac{W^{1/3}}{{Z_o}^{1/3}}\right) \tag{9}$$

The value of $Z_o = (D + 9.8)$ corresponds to the hydrostatic pressure, at the location of the explosion. The time to obtain the maximum radius writes:

$$T = K6 \left(\frac{W^{1/3}}{{Z_o}^{5/6}}\right) \tag{10}$$

For the equation previously described there exist some data that can help to obtain the equivalent equations for other type of explosives. This are called the similitude equations.

Table 1 Equivalent coefficients, available from: (Reid, 1996)

	Coefficient	HBX-1	TNT	PENT	NUCLEAR
Shock-wave	*K1*	*53,51*	*52,12*	*56,21*	*1,06E+04*
Pressure	*A1*	*1,144*	*1,18*	*1,194*	*1,13*
Decay	*K2*	*0,092*	*0,092*	*0,086*	*3,627*
Time-Constant	*A2*	*-0,247*	*-0,185*	*-0,257*	*-0,22*
Impulse	*K3*	*7,263*	*6,52*	*6,518*	*4,50E+04*
	A3	*0,856*	*0,98*	*0,903*	*0,91*
Energy Flux	*K4*	*106,8*	*94,34*	*103,11*	*1,15E+07*
Density	*A4*	*2,039*	*2,155*	*2,9*	*2,04*
Bubble Period	*K5*	*2,302*	*2,064*	*2,098*	*249,1*
Bubble Raious	*K6*	*3,775*	*3,383*	*3,439*	*400,5*

2.1.1. Gas bubble parameters

As it is mentioned by (Hsu, Liang, Nguyen, & Teng, 2013), ignoring the surface tension and the viscosity, the bubble boundary momentum equation can be written (Rayleig, 1917):

$$R_b\ddot{R}_b + \frac{3}{2}\dot{R}_b{}^2 = \frac{P(R_b) - P_\infty}{\rho_l} \tag{11}$$

Where R is the radius of the bubble, $\rho_l$is the liquid density, P_∞ is the pressure in the liquid at infinity, and $P(R)$ is the pressure in the liquid at the bubble boundary. Considering the effects of viscosity and the surface tension the equation is deduced by (Plesset & Prosperetti, 1977) and is stated as:

$$R_b\ddot{R}_b + \frac{3}{2}\dot{R}_b{}^2 = \frac{1}{\rho}\left\{p_i - p_\infty - \frac{2\sigma}{R} - \frac{4\mu}{R}\dot{R}_b\right\} \tag{12}$$

The variable σ represents the surface tension constant and the liquid viscosity coefficient. The p_i variable is the pressure at the bubble wall and p_∞ is the pressure at infinity. Considering the rapid effect of the explosion that is (about 1 second), the heat exchange is negligible, and the Rayleigh-Plesset equation is usually expressed using the following notation:

$$R_b{}'\ddot{R}_b{}' + 1.5\dot{R}_b{}'^2 = \varepsilon\left(\frac{R_b{}'_0}{R_b{}'}\right)^{3\gamma} - 1 \quad (13)$$

R' is the dimensionless radius of the bubble, R'_0 is the initial dimensionless radius of the bubble, γ is the special heat ratio, and ε is the strength parameter (the ratio of the initial bubble pressure to the ambient pressure).

As is mentioned by (Prior & Brown, 2010) a more accurate approximation to determine the period of the bubble is:

$$T_1 = K\left(\frac{W^{1/3}}{(Z_1 + 10.1)^{5/6}}\right)\left(1 - \frac{R_1}{5\,Z_1}\right) \quad (14)$$

The term *K* is a factor determined by the type of explosive used, *W* is the charge weight in kilograms, R_1 is the maximum wave radius and Z_1 gives the depth of the explosion. The second term helps to add the influence of the sea surface on the bubble oscillations. R_1 can be obtained by:

$$R_1 = \left(\frac{W}{Z_1 + 10.1}\right)^{1/3} \quad (15)$$

It is also important to mention that the ratio of the second period to the first one is:

$$\frac{T2}{T1} = 0.7 \quad (16)$$

2.1.2. Shock factor (SF)

As points out by (Keil, 1961) , since there are many case scenarios at which an UNDEX might take place, the severity of the attack can be catalogued by the Shock Factor (SF), which takes into account the standoff distance, the power of the explosive, the relation between the shock velocity and geometry of the ship and charge location.

The attack severity is measured by the SF which can be written as:

$$Maximum\ SF = \frac{W^{1/2}}{R} \quad (17)$$

According to (Liang & Tai, 2006), if one takes into account the angle of incidence of the shockwave the previous equation writes:

$$SF = \frac{W^{1/2}}{R}\left(\frac{1+\cos\theta}{2}\right) \tag{18}$$

Figure 2 extracted from (Liang & Tai, 2006) shows the geometry lay-out of the problem, and how the shock wave angle and stand-off distance are considered.

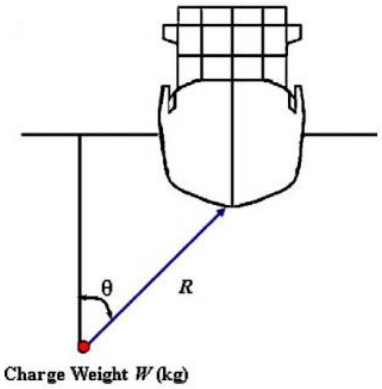

Figure 2 geometry layout of the charge location respect to the vessel. Available from: (Liang & Tai, 2006).

As it is mentioned by (Reid, 1996), the shock factor should be taken with care, as for example a small charge near the hull can give the same shock factor than a bigger one located further. However, the big charge will have a longer impulse time which might create a bigger damage to heavier items of equipment. Similarly, the effect of the local charge with the same SF, will induce a bigger bending moment due to its smaller curvature and to the difference between the lead time at the fore and aft, compared to amidships.

Later, it will be shown that this value gives a small glimpse on the level on the power of the explosion, but for a better understanding, it is necessary to know the stand-off distance and the weight of the charge to perform an appropriate analysis.

2.1.3. Shock spectrum

According to (Alexander, 2009), the shock spectrum is one of the most powerful tools to analyze the behavior of mechanical systems, allowing for the analysis of its response to an acceleration input. This tool is used to characterize the frequency response of shock environments and to estimate the maximum dynamic response of mechanical system. As shown in Figure 3, the shock time response signal can be characterize in two main regions: the primary region is the response of the system while the shock wave is still emitted and the second one corresponds to the residual part of the signal. The maximum amplitudes usually take place in the primary region, whilst it tends to be lower in the secondary one.

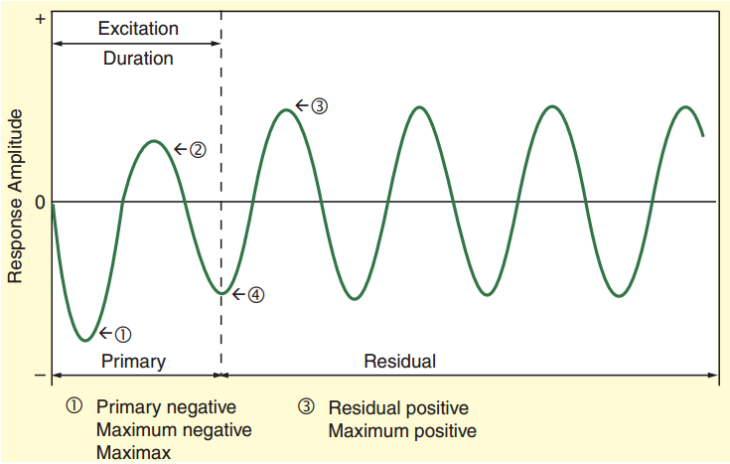

Figure 3. Time domain response signal. Taken from (Alexander, 2009).

The (ISSC, 2006) report mentions that the importance of the dynamic effects depends on the rate of change from the dynamic properties of the structure, i.e. its natural frequencies, modal shapes and modal damping factors.

During a shock trial on a ship, a series of instruments are attached at critical points of the ship, to capture the time domain signals such as displacements, speeds and accelerations at critical points. Figure 4 shows a time domain signal captured at the inner bottom:

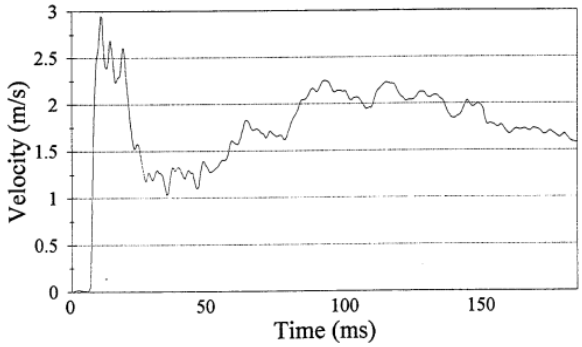

Figure 4 Shock velocity signal obtained at the inner bottom. Taken from (Reid, 1996)

According to (Reid, 1996), when the lower part of a surface ship is stroke by a shock wave, the higher amplitudes are measured at the ship bottom. The shock then travels along the whole structure, and its amplitude tends to decease when the height of the bulkhead sensors increases (see Figure 4). This situation lies on the fact that a ship is not a complete stiff structure, and does not instantaneously transmit the accelerations. Away from the bulkheads, the measured accelerations obtained are different, and their magnitudes dependent on the sections and deck stiffness. As a rule of thumb, large displacements are characterized by low frequencies, and small displacements are characterized by high frequencies.

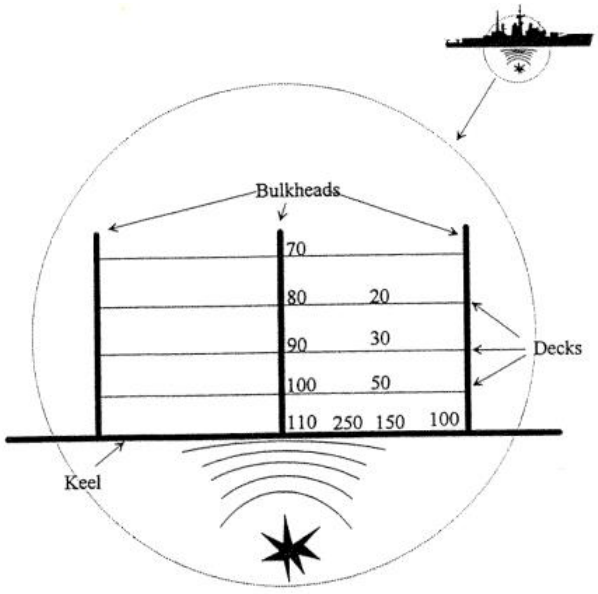

Figure 5. Example of the different accelerations obtained at different bulkheads heights; taken from (Reid, 1996).

Once the signal is obtained, it should be correctly treated and then converted into the frequency domain in order to obtain the response spectrum. Figure 6 shows the typical response spectrum obtained from a shock signal, illustrating at the same time the displacement, velocity and

acceleration. The damage potential of a shock pulse on an equipment increases as the displacement, velocity or acceleration increases. The magnitude of the response in the spectra provides a measure of the shock damage as a function of frequency.

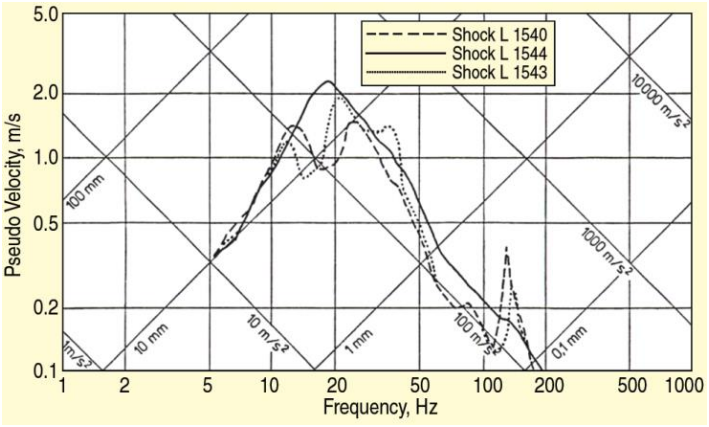

Figure 6 Frequency spectrum from different shocks, taken from (Alexander, 2009).

2.1.4. Other effects

According to (Mehaute & Wang, 1996), when an underwater explosion occurs near the free surface, a water effect occurs: once the bubble is created and starts to contract, the water near the bottom of the bubble will flow inwards faster than the water at the top or the middle; this will create a flow that will surge passing through the top of the bubble, resulting plumes that are usually seen at the surface. Figure 7 shows the detail of this water effect.

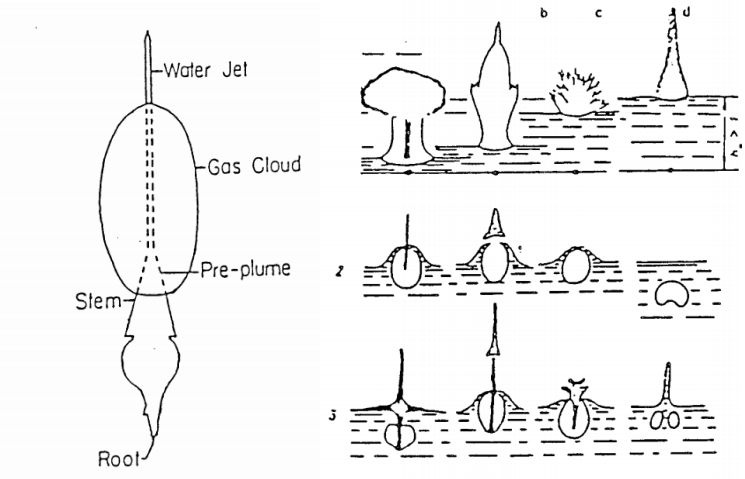

Figure 7 Water jet effect near the surface, and the different plume like patterns, taken form: (Mehaute & Wang, 1996).

Usually the effect of the bottom during an UNDEX is the reflection of the wave acquiring additional damage capacity; this wave has a compressive nature. The effect of an UNDEX near the free surface is that the shockwave will be diffracted causing cavitation over the surface of the water. The reflection of these waves with bottom and free surfaces will create an overlapping with the main shockwave, increasing the vessel's potential damage due to the explosion.

Another interesting effect observed in an UNDEX, is the bubble migration that occurs once the first pulsation is completed. This phenomenon is observable on the high speed video performed by (Edgerton, 1943). In the same experiments, it is also possible to see the attraction effect that a near surface will do to the pulsating bubble.

Figure 8 extracted from (Hollyer, 1959) shows the effect at point T of the shockwave reflection on the free surface.

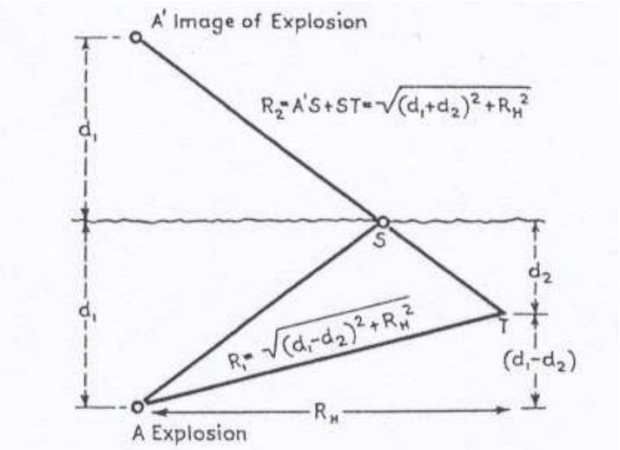

Figure 8. Schematic of the geometry of the surface, for a load at point A and measured at point T.

The effect of the reflection at this point modifies the usual decaying shock pressure signal and instead, creates the signal obtained at Figure 9. In this case, the effect of the reflection leads to a situation where the point T, instead of being in compression, is found in tension.

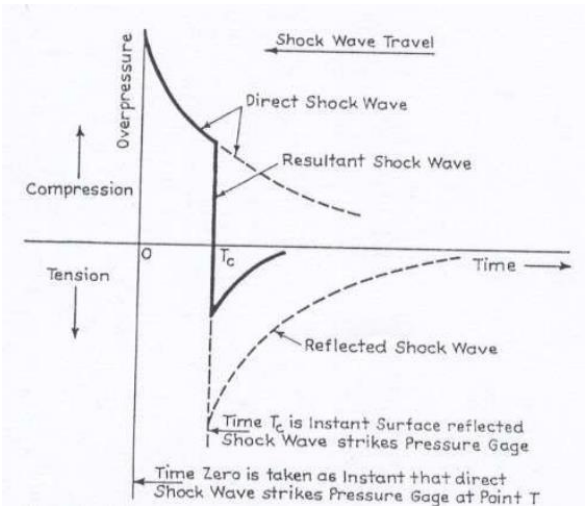

Figure 9. Pressure time signal measured at point T, taken from: (Hollyer, 1959).

2.2. Effects over a surface ship (typical damages)

Taking all the phenomena previously discussed into account, it is important to analyze the main effects over a ship. There are many case scenarios that can achieve significant harm to a vessel. This is for instance, from the effect of direct contact with the charge, or the effect on vital equipment of the vessel, sensible to abrupt change of speed or acceleration. The following content will show some of the main effects that an UNDEX can produce on to surface vessel.

2.2.1. Blast damage

As it is exposed by (Keil, 1961), the typical damages found on a structure are generally, dependent on the distance from affected model, defined as the stand-off distance, the orientation of the vessel, the depth of occurrence of the event and the amount of power of the explosive used.

The closer is the event to the ship, the more damage might occur. An example of close impact is the one that happened to the USS Cole destroyer, by a bomb carried by a small vessel that got close to the destroyer (Figure 10). The attacked produced a 10 meter hole at port side, and the loss of 17 crew members.

For this kind of explosions that occur near the surface, the main failure is produced by the blast itself rather than by the interaction with the fluid.

Figure 10. USS Cole detail of the damage. Available from: (NAVY, 2015)

For a close impact, the affected area, will largely deform, reaching the breaking point and affecting the structural integrity of the vessel. As an example, if the blast is produced near the center of the vessel, where higher stresses are present, there is a high probability for it to sink, as it can decreased the overall hull bending moment capacity of the structure, but also by the loose of water-tightness of the bulkheads.

As the charge is moved away, the effects over the vessel are diminished. The closer the charge, the higher the intensity, reaching the breaking point of the material. A step further will create permanent (plastic) deformation, and finally a larger standoff will only produce elastic deformation.

2.2.2. Whipping response

In order to talk about the whipping response, making reference to (Clements, 1972), it would be important to mention first, that a structure has a number of degrees of freedom. Each natural frequency is a property of the entire structure, and individual parts of the structure will contribute more than others. Each mode of vibration of the structure is characterized by a natural frequency and a mode shape. The natural frequencies and mode shapes are the eigenfrequencies and eigenfunctions of the characteristic equation of the structure.

As mentioned by (DeRuntz Jr, 1994) the whipping effect occurs when the bubble pulsation matches one of the low order eigenfrequencies of the ship; in order words, when the lower frequency modes of the structure are excited. This kind of effect is more dangerous for a ship rather than for a submarine; this is due to the fact that the structure of the ship is free to move upwards, whilst as a submerged submarine the structure would be damped due to the water surrounding the structure (Reid, 1996). As (Keil, 1961) mentions in his paper failures usually happen at the lower flange of the hull girder. As a result of the initial loading produced by the bubble as well as the second later oscillations, the hull girder may deform in compression at a higher level than its buckling limit. This effect is usually considered by only taking into account the later pulsations for the analysis. Figure 11 illustrates the whipping effect on a ship structure.

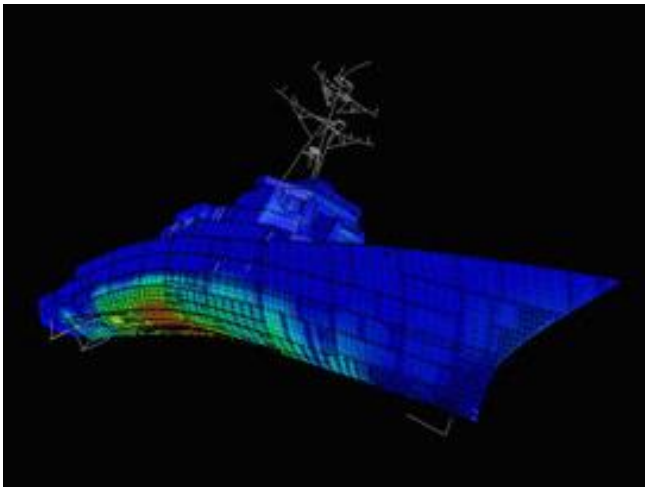

Figure 11. Whipping effect, available from: http://www.nps.edu/svcl/subPages/Projects.html

2.2.3. Water jet effect

As mentioned early by (Reid, 1996), the collapse of the bubble usually creates a sudden water flow, that if occurred near the hull, it can penetrate the bottom of the ship causing large damage. The resulting flow can reach speeds in the range of this 130-170 m/s. Figure 12 it can be seen an approach of the effect during the bubble collapse:

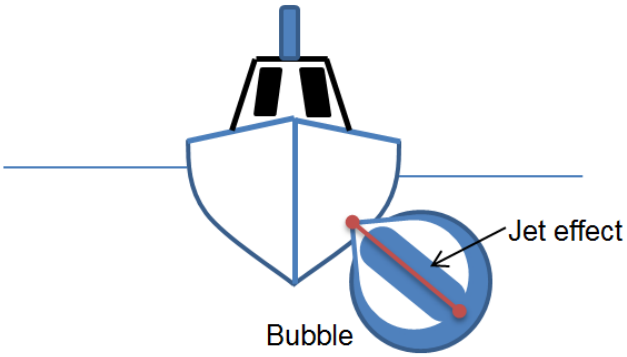

Figure 12 Jet effect produced by the collapse of the bubble.

2.2.4. Effects on machinery and equipment

The shock is usually transmitted along the structure causing the surface ship to move upwards (Reid, 1996). The shockwave will travel along the ship structure, reaching the different bulkheads of the ship. Since these latter are one of the most rigid parts, they will serve as an excellent conductor of the shock.

This enormous amount of energy, may damage many parts at the ship, such as machinery and equipment, damaged by the high peaks of acceleration and speed. The high frequencies associated to the shock can be a source of damage for pumps switch boards, generators, electronic components, etc. Figure 13 presents typical shock resulting signals at a point of the ship structure.

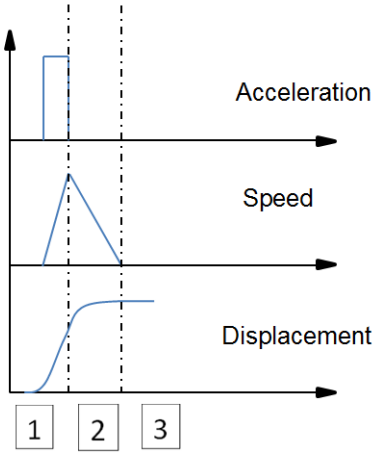

Figure 13. Pulse effect in a point over the structure.

During this event, three periods can be distinguished. During the first one, failures can happen due to the large accelerations at low displacements. At this point, brittle failures can occur in equipment with foundations made out of cast iron or cast aluminum, and also where shearing appears in bolted connections.

The second period is characterized by a deceleration and large displacement causing tensile failure of welded components. The third period is characterized by large displacements due to the inertia gained by the equipment embarked onto the ship, although the source of motion has stopped. Typical failures found are the bending of structural elements or impacts between parts and equipment.

2.2.5. Effects on suspended materials attached to resilient mountings

According to (Clements, 1972), one way to isolate the embarked components loaded onto a ship consists in adding resilient mountings. These systems, often called shock mounts or vibration isolators, have the function to act as a seismic suspension and to protect the equipment that they are beholding from a shock. These isolators are designed to minimize the equipment's motion, to limit the magnitude of impulsive forces transmitted to it, and at the same time, accompanied with the correct clearance, to avoid that the supported equipment crashes its surroundings once it is displaced by the shock.

Shock isolators come in different varieties, to fit each of the design criteria. In this case it is important to be cautious at the moment of performing the design. Adding a resilient mounting to a piece of equipment with negligible mass will generate a soft spring effect between the equipment and the structure. However, when its mass is not negligible, the equipment can act as vibration absorber for the resilient mounting. Examples of resilient mountings are shown in Figure 14.

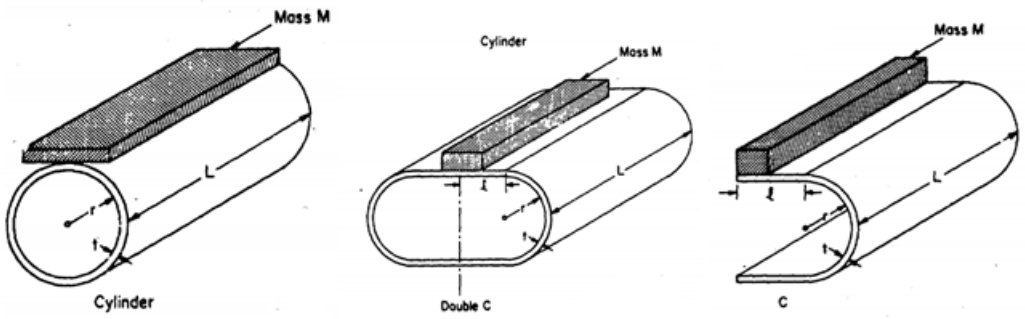

Figure 14. Resilient mountings examples, taken from: (Keil, 1961).

As shown by (Keil, 1961), the shock design of the isolation system for a shock, should take into account the following points:

a) The dynamic response of the equipment, and its foundations, considering the dynamic properties of the materials.

b) The shock environment at which the piece of equipment would be subjected.

c) The fact that the theoretical design approach should be sufficient, knowing that in some cases experimental testing is needed.

(McCarthy Jr., 1995) initiated the analysis of suspended materials inside the ships by the so called Dynamic Design Analysis Method (DDAM). The design stage consists in representing the equipment or equipment or structure by an equivalent mass-elastic system, (see Figure 15), and designing the system to sustain dynamic stresses by shock response motions. By solving the equations of motion of this mass-spring system, resulting forces and displacements are used to determine the stresses and deflections of various components of equipment. Finally, these values are compared with specified allowable values to verify the acceptability from a shock standpoint.

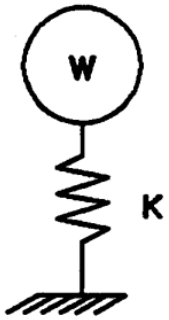

Figure 15. Single degree of freedom foundation, taken from (McCarthy Jr., 1995).

2.3. Simulation strategies and validation tools

In order to correctly execute a simulation of an UNDEX, it is necessary to take into consideration the simulation as a chain of events, which are: explosive detonation, pressure wave propagation, fluid structure interaction, and finally the structural response (ISSC, 2006). The fluid structure is one of the topics that has been mostly studied to obtain a good simulation results. One way is to use the Double Asymptotic Approximation (DAA) (DeRuntz Jr, 1994) which consists in modeling the surrounding fluid as a membrane on the wet surface in contact with the fluid.

Some of the codes that include the fluid-structure interaction effects associated to an UNDEX are LS-DYNA, AUTODYN, NASTRAN, ABAQUS, etc. To get a general insight of what are the general equations that act during this sort of simulations, the general equation acting on a flexible structure writes (Nu, Zhi, & Wepeng, 2014):

$$M\,\ddot{X} + C\,\dot{X} + KX = F \tag{19}$$

Where *M*, *C* and *K* are refereed as the mass, damping and stiffness matrices of the model, and F denotes the external forces the degrees of freedom of the structure being analyzed. The variables $\ddot{X}$, $\dot{X}$ and X, represent respectively the acceleration, velocity and displacement vectors of the nodes which compose the finite element model of structure. The source of excitation *F* for a submerged structure can be expressed by the help of acoustic flow as:

$$F = -GA_f\,(p_i + p_s) \tag{20}$$

Where p_i and p_s, represent the nodal wet surface nodal pressure referring respectively to the incident flow and scattered flow. The value A_f is the diagonal matrix associated with an element in the fluid mesh, and *G* represents the transformation matrix relating the structural fluid and nodal surface forces.

The interaction between the fluid and the wetted surface of the vessel is modelled by the so-called Double Asymptotic Approximation (DAA) (DeRuntz Jr, 1994); based on acoustical differential relations between the fluid pressure and its velocity on the surface of a submerged structure, uncoupling the motion of the structure from the motion of the fluid. The fluid loading is equivalent to a damping force at early time and an added mass at later time:

$$M_f \dot{P}s + \rho c A_f ps = \rho c \, \dot{u}_s \tag{21}$$

M_f is an (*N* x *N*) fluid mass matrix, where *N* if the number of degrees of freedom ρ and c are the fluid density and the sound speed in the fluid respectively and u_s is the velocity of the fluid particles normal to the structural surface. Structure and fluid speed vectors are relied by the following equation:

$$G^T \dot{X} = u_i + u_s \tag{22}$$

Where u_i is the speed of the incident flow. Using equations 0 and 0 as the same way as 0 and 0, the coupled fluid-structure interaction equations can be written:

$$M_s \ddot{X} + C_s \dot{X} + K_s X = -G A_f \, (p_i + p_s) \tag{23}$$

$$M_f \dot{P}_s + \rho c A_f Ps = \rho c (G^T \dot{X} - u_i) \tag{24}$$

2.3.1. Simulation of stiffened panel to shock wave

One of the ways to validate the simulations of an entire UNDEX without reaching high costs is to perform small tests on panels. As an example (Zong, Zhao, & Li, 2013) develop experiments on panels subjected to UNDEX, and compare experimental results with the simulations based

on ABAQUS, taking into account the fluid structure interaction (FSI). Figure 16 shows the great similitude between the simulation and the actual experiments.

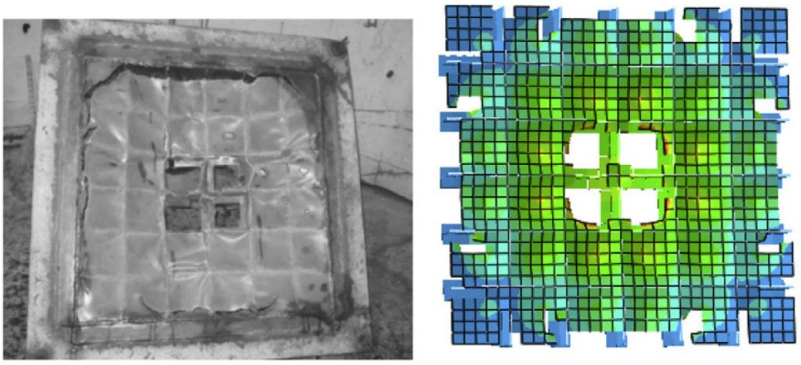

Figure 16. UNDEX event test and simulation comparison of a stiffened panel. Taken from: (Zong, Zhao, & Li, 2013).

According to (Gupta, Kumar, & Hegde, 2010), usually when a plate is subjected to an UNDEX, there usually exists three types of failure criteria regarding the plates:

Failure mode I: the plate will experiment large plastic deformation.

Failure mode II: Once plastic deformation occurs, a tensile tearing appear at the central borders of the plate, and then propagate to the borders. Within these failures it is found two modes: partial tearing with increased midpoint deformation and decreased midpoint deformation. For thin plates, according to (Ramajeyathilagam & Vendhan, 2004), the effects of the plastic hinge should be also modeled to have an accurate solution. Large number of elements will be necessary to predict the edge tearing; where the calculated effective plastic strain at the edge (ε_{eff}), given by the expression below, exceeds the rupture strain (ε_{rup}).

$$\varepsilon_{eff} = \int_0^l \left(\frac{2}{3}\dot{\varepsilon}_{ij}^p \dot{\varepsilon}_{ij}^p\right)^{1/2} dt \tag{25}$$

Where $\dot{\varepsilon}_{ij}^p$ is the plastic strain rate.

Failure mode III: This shearing failure mode occurs bolted plates if the shear stress at the edge of the plate (τ_e) exceeds dynamic ultimate shear strength (τ_{dult}) given by:

$$\tau_{dult} = \frac{\sigma_{ult}}{\sqrt{3}} \left(1 + \left|\frac{\dot{\varepsilon}}{D}\right|\right)^{1/n} \tag{26}$$

Where (σ_{ult}) is the ultimate strength of the material.

According to (Ramajeyathilagam & Vendhan, 2004), the failure modes II and III, do not occur independently and their interaction may be described by one of the following criteria: the linear criterion interaction (LIC) and the quadratic criteria interaction (QIC):

$$\text{LIC:} \quad f = \left|\frac{\varepsilon_e}{\varepsilon_{rup}}\right| + \left|\frac{\tau_e}{\tau_{dult}}\right| \tag{27}$$

$$\text{QIC:} \quad f = \left(\frac{\varepsilon_e}{\varepsilon_{rup}}\right)^2 + \left(\frac{\tau_e}{\tau_{dult}}\right)^2 \tag{28}$$

Where ε_e is the total strain at the edge of the plate.

According to (Elsaye, Hui, Lili, & Mahmoud, 2014) behavior of a stiffened panels allows also to quantify the effect of the strain rate of the material as well as the rate of structural (hysteresis) damping. The models presented on their work use of the package ABAQUS and include the fluid structure interaction. This study presents the analysis of different configurations of steel stiffened panels using a performance improvement ratio, that is, a ratio that compares the performance un-stiffened panels and panels with different stiffening configurations.

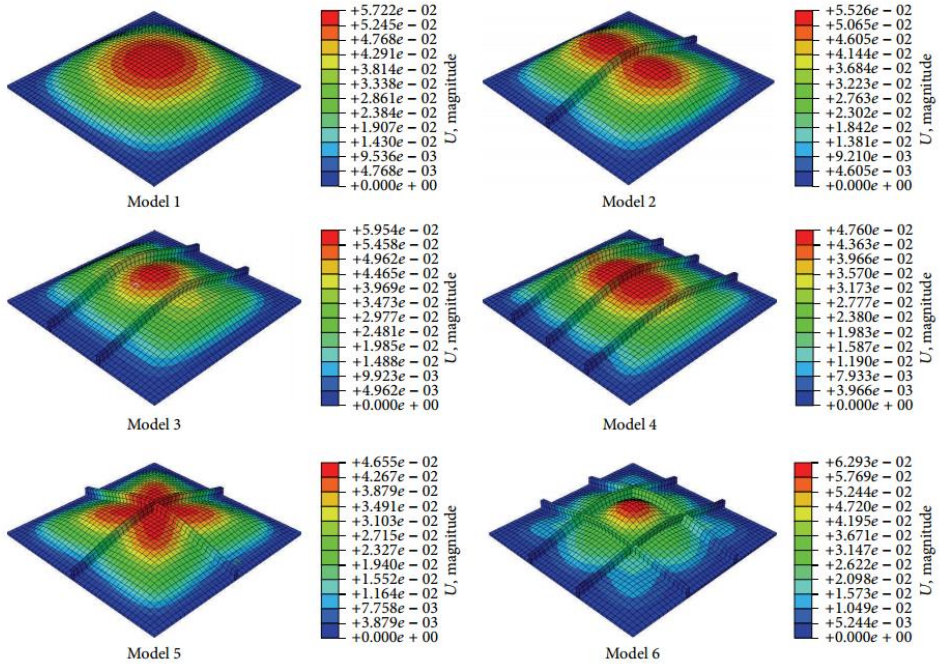

Figure 17. Magnitude of deformation of the different stiffened panels being used. Available from: (Elsaye, Hui, Lili, & Mahmoud, 2014).

2.3.2. Full ship simulation and modelling

According to (Ding & Buik, 2015) many approaches are available to simulate the effect of an UNDEX. For instance, some simplified approaches do not take into account the fluid structure interaction, but instead use the scattered pressure history; calculated by means of theoretical formulations and applied to the structure. This is a really rough approach that only will help to obtain an overview of an initial predesign procedure. To obtain more realistic results, it is important to take into account the fluid structure interaction where effects such as cavitation or deformation of the hull have to be accounted for. Figure 18 highlights the general procedure involved during the development of a simulation.

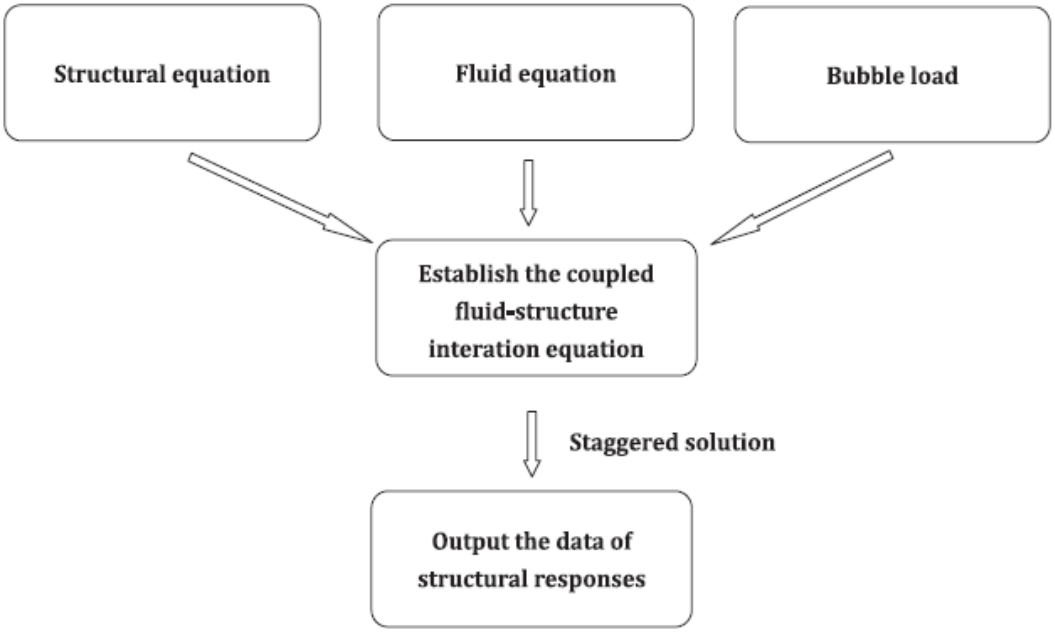

Figure 18. Flow chart of general calculation procedure for a simulation of an UNDEX. Taken from (Nu, Zhi, & Wepeng, 2014).

Up to now, many tools are available to simulate the effects of an UNDEX onto a submerged structure (Miller, Jasak, Boger, Paterson, & Nedungadi, 2012), based on different approaches such as: compressible multi-fluids method, free Surface flows method, volume of fluid method, level sets method, segregation/Projection methods for multi-phase flows, meshless methods based on smoothed particle hydrodynamics (SPH) and incompressible two-phase methods.

Since the modelling of a full ship will be very time demanding, the structure of the ship is often constructed using simplified elements such as shell elements, and the loads or masses of the equipment are modeled using lumped masses distributed on one or several nodes. Figure 19 presents the different meshes used for a hydrodynamic model, including the connecting layer between the structure finite element mesh and the fluid mesh.

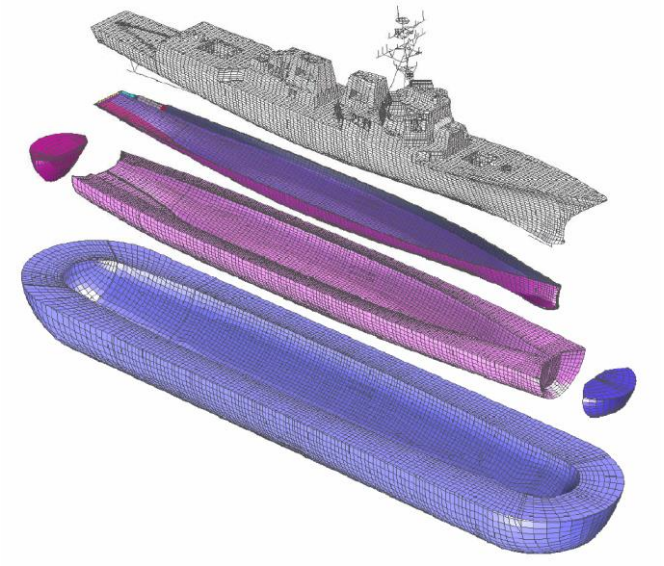

Figure 19. Exploded fluid mesh model, taken from (Didoszak, Shin, & Lewis, 2001).

Using the previous validated evaluation of the stiffened panels, (Zong, Zhao, & Li, 2013) performed large simulation of an entire ship using different standoff distances. The charge being used for the simulation is 200 Kg TNT, and the standoff distances are varied between 10 to 5 meters. Figure 20 shows the different modes of failure obtained.

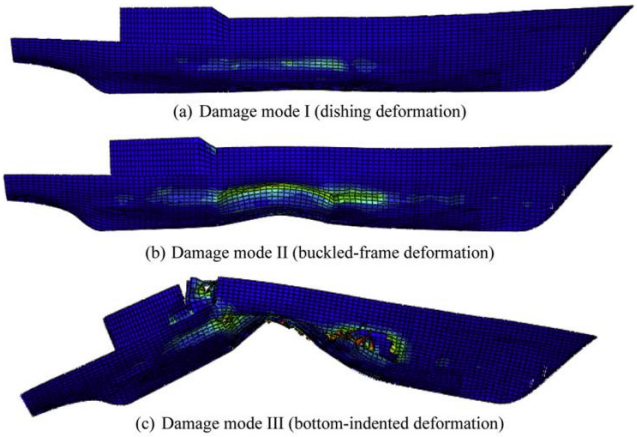

Figure 20. Different failure modes produced by different charges at different stand-off distances.

2.3.3. Use of simulation to validate the use of new materials

According to (Elsayed, Hui, Lili, & Helal, 2014), the use of fiber reinforced composites is now quite regular for naval applications, such as the design of hulls and submarine components. The advantages are long fatigue life, improved corrosion resistance and reduced maintenance costs.

In the mentioned work, the model is elaborated using ABAQUS software and includes the fluid structure interaction. ABAQUS and ANSYS codes are successively used to explore and optimize the composite layout regarding the structure UNDEX behavior. The Tsi - Wu failure criteria is used and time history data of displacement and velocity are post-processed at different points on the structure. Different simulations are carried out by changing the charges and the different stand-off distances, in order to determine the maximum shock factor that the structure can withstand. Figure 21 shows the results of different acoustical pressure magnitude (POR), generated by different charges at a stand-off distance of 8 meters.

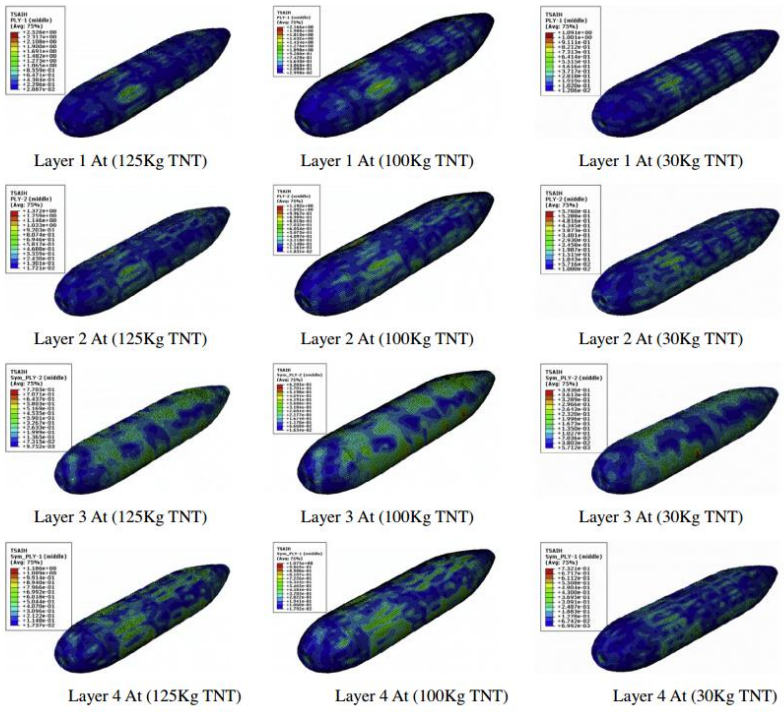

Figure 21. Acoustical pressure magnitude of the different layers used in the model, taken from (Elsayed, Hui, Lili, & Helal, 2014).

(Chul-Hong & Young S., 2012) investigate several techniques to reduce stresses by performing simulations on submerged panels. These panels use different type of materials as rubber backed plates from 1 to 3 centimeters of thickness, as well as sandwich panels based on square, or octagonal cells. They obtained a considerable reduction on deformation and average stress levels as compared to a single plate. This study also includes the optimized dimensioning of the panels in terms of strength weight ratio, and present a set of formulas to determine the thickness of the materials used to achieve a certain level of stresses. Figure 4 shows a time history of the

stresses on a sandwich plate structure, as well as the different set of honeycomb tested configurations.

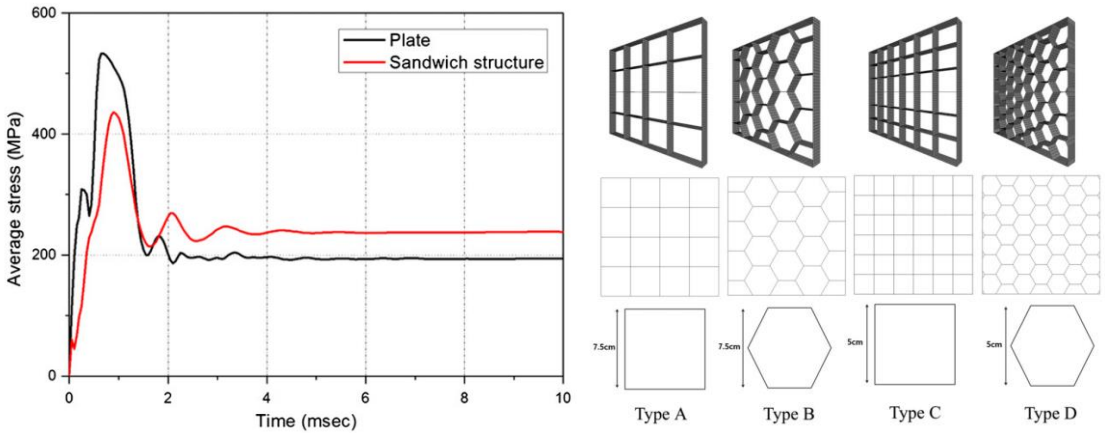

Figure 22. Sandwich structure plate response to an UNDEX, taken from (Chul-Hong & Young S., 2012).

Another investigation that confirms the great advantages of sandwich panels, the use of elastic coating and honeycomb configurations, has been presented by (Feng, Yong, Yu, Hongxing, & Dawei, 2014). Their experiments on a honeycomb structure panel with different explosives and locations confirm the reduction of deformations and strains obtained by the use of these configurations. The properties that are required are resistance, resilience, and at the same time great acoustic impedance mismatch.

2.4. General review of existing rules regarding explosions

The following content is a general summary of the main rules that are now available for the design of structures against the shock produced by an UNDEX event. In general there are some particularities within the rules that unified the way a design problem is defined. In fact, the procedure will be highly dependent on the failure criteria established for the ship components, which will also depend on the ship functions, and to some extent to the bearable costs that a particular vessel will have.

As it has been described before, there are many tools which are available to analyze the UNDEX problem regarding the design; but in general a shock analysis procedure is chosen according to the design stage of the project. Figure 23 shows a general overview of the procedures that are required to be performed.

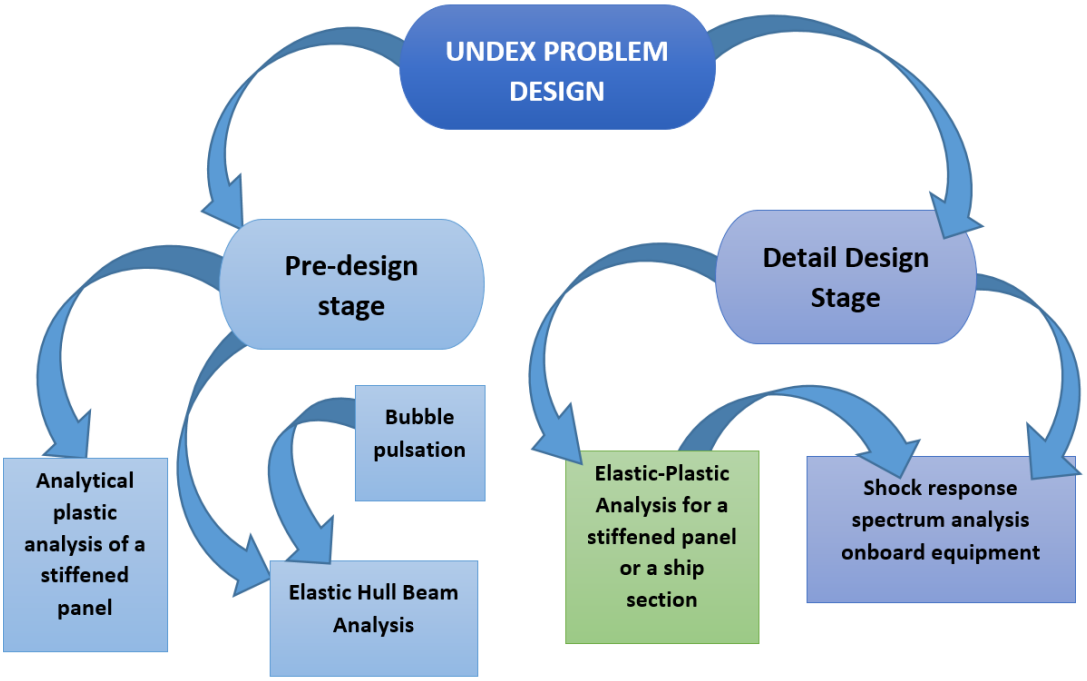

Figure 23. General overview procedure for UNDEX analyses.

The following part of the document is a summary of the available accessible documentation from different sources which are a guide to perform the ship shock analysis of naval surface vessels.

According to (NRL, 1965), the purpose of any program of shock analysis, design and testing is to be able to perform their intended functions during, and after severe environmental conditions. It is obvious that a direct hit by a weapon will perpetrate significant damage to a ship in the immediate region of the explosion. Therefore the main efforts are focused on the damage generated by a weapon at the immediate region. That's why when the mechanical shock loading is transmitted to: machinery, equipment's, and other structures, the main interest is to ensure their survivability.

2.4.1. Requirements for shock protection

The decisions regarding the degree of protection required must fulfill the conditions on how effective a ship and its composing system will resist, when an event of this characteristics appears. For instance, when a ship is subjected to an UNDEX, there will be some systems which will have the highest role ensuring the operation of the vessel, while others will only act as not

vital items. In this order of ideas, it is important to have a proper classification on the equipment onboard, ensuring that vital equipment should be able to deliver the proper operation.

2.4.2. Selection of failure criteria

The failure criteria in shock test are very simple, and are relied on the fact that equipment can still perform its useful function, and must be associated to a value that can be calculated.

The shock induced failures can be classified in “mechanical”, “functional” or “secondary”.

- Mechanical failures can be associated with excessive flexibility, in that strains have become too large.

- Functional failures are the ones that produce and intermittence in the delivery of a service, and can be reestablished or corrected once the incident is over.

- Secondary failures are the ones caused by some other piece of equipment that due to its movement affects a vital piece of equipment causing its failure.

All this types of considerations are needed to be taken into account in order to define a failure “indicator” associated to the components subjected to a UNDEX and to make even clearer for the designer the importance of the definition of failure indicators which are:

- Allowable stresses or strain.
- Allowable internal forces and moments.
- Allowable displacements, relative and absolute.
- Allowable energy absorption.
- Allowable absolute accelerations.
- Allowable bearing loads.

It is worth noting that shock design analysis alone is rarely applicable if an assemblage of items is so complex that a reasonable analysis of each component is impossible or prohibitively expensive.

2.4.3. Development of analysis and design procedures

Usable design information should be classified in order to be accessible and easy to use by the designer of the shipboard equipment. The design engineering process should also be as practical as possible, so that it is not limited to a certain amount of specialists. At the same time, unrealistic or unachievable goals must also be defined, so energy and time is not invested, and an alternative solution should be found. Any practical shock design method should have several levels easily recognizable requirement or characteristics:

1. Shock protection design levels should be stated depending on the importance on the onboard equipment.
2. A description of the environment at which the piece of equipment should survive must also described.
3. There must be some means of describing the item to be analyzed in a mathematical form.
4. A set of standard mathematical techniques should be available, so that the design can be analyzed quickly and by the use of software and with some degree of uniformity using various numerical codes.
5. There must be defined failure criteria for each studied item which can be determined from the analysis of the item itself and its environmental conditions.
6. The technique should serve as a learning tool so that additional similar items will be analyzed each time faster
7. Finally, design is an iterative procedure relying on past experience and available design rules. Stresses, deflections and bearing loads cannot be determined until a design has been assumed. If stresses are too high, then the design must be modified.

All of the information previously discussed is not enough, and needs a deeper review by all of the personal involved in the design process.

2.5. Shock design methods for embarked materials.

2.5.1. Shock Design Numbers

In the shock design number approach, the design input is specified by a so-called "Shock Design Number", proposed by the "American Bureau of Ships (BuShips), which varies with the gross weight of the equipment, with the type of ship, and with the direction of the attack. The equipment weight times the appropriate design number gives a static force which is applied at the center of gravity of the equipment prior to a static analysis. Loads in 3 orthogonal directions are applied individually, without superposition of any other stresses. The performance standard is the yield strength of the material.

So far, although this very rough approach has been very popular its simplicity, it is an erroneous approximation because the flexibility of the different installations (supporting systems like decks, etc.) is ignored, as well as the integrity evaluation of internal components.

Some variations of the design number procedures have been proposed for surface ship installations. In those approaches, larger shock design numbers than those proposed by BuShips, are defined from short accelerations, measured from velocity records. A "resiliency factor", based on peak shock spectra is also introduced. It modifies the shock design number in accord with the ratio of the dominant frequency of the item to the shock disturbing frequency of the general input motion. The shock design number and resiliency factors are obtained from "envelope-type" analyses of available test information on surface ships. In this case the yield stress is used as the failure criteria. The accuracy of the describe procedure has not yet been validated.

The proposal of a shock criteria using the envelop method was used before, until the "spectrum-dip" effect was found, showing that this criteria may lead to a very conservative design.

2.5.2. BV043/85 German rules for embarked equipment to high impact

One of the techniques that have been used to calculate the shock response spectrum is the one used the by Germany ((BV), 1973) it refers to the military specifications for high impact mechanical shock applied to onboard equipment, and is typically used as a reference in Naval

projects by customer demand. The shock response is specified by the customer, which usually comes with a defined constant displacement D_0, a defined constant velocity V_0 and a defined constant acceleration A_0 (Xiong-liang, Qi-xin, A-man, & FENG, 2008). Figure 24 shows the regular specified shock spectrum given for equipment.

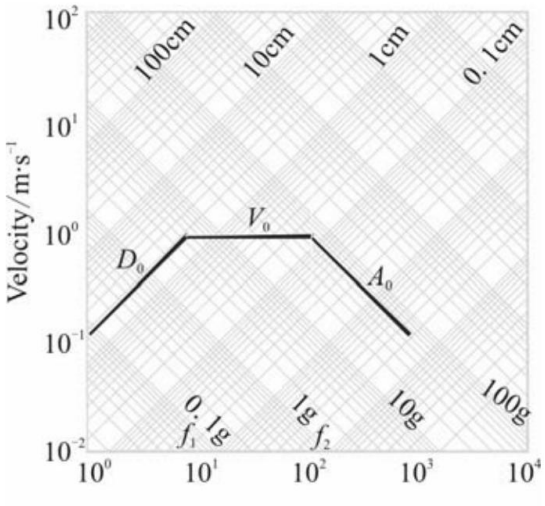

Figure 24. Typical shock response spectrum given for equipment, available from (Xiong-liang, Qi-xin, A-man, & FENG, 2008)

Based on this spectrum which is handled by the customer the time history acceleration signal is constructed; following a triangular wave, which is applied the equipment foundations. Figure 25 shows the typical wave pattern applied. The frequency range of the spectrum can be calculated using the following formulas:

$$f_1 = V_0/2\pi D_0 \tag{29}$$

$$f_2 = A_0/2\pi V_0 \tag{30}$$

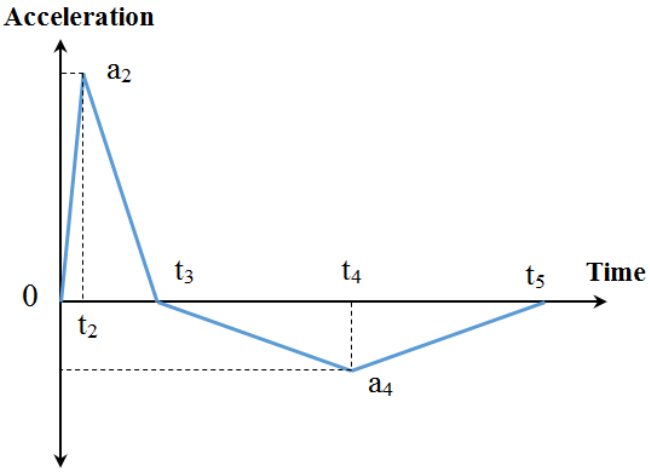

Figure 25. Acceleration shape signal. Available from: ((BV), 1973)

The following formulas specify the parameters that need to be calculated in order to construct the triangular signal:

$$a_2 = 0.6 \cdot A_0 \tag{31}$$

$$t_2 = 0.6 \cdot \frac{V_0}{a_2} \tag{32}$$

$$t_3 = 1.5 \cdot \frac{V_0}{a_2} \tag{33}$$

$$t_5 = \frac{6 \cdot d_0 \cdot 1.05 - 1.6 \cdot a_2 \cdot {t_3}^2}{1.6 \cdot a_2 \cdot t_3} \tag{34}$$

$$a_4 = a_2 \cdot t_3/(t_5 - t_3) \tag{35}$$

$$t_4 = t_3 + 0.6 \cdot (t_5 - t_3) \tag{36}$$

One of the ways to estimate the values of values is proposed by (Tao, 2009) can be done by the use of the dynamic analysis method (DDAM) later explained in this document, which defines a method to construct a shock spectrum for an equipment, and obtain the values D_0, V_0 and A_0.

For the case of the sinusoidal signal which usually takes the function usually seen in Figure 26. The equation that represents the signal writes:

$$a(t) = \begin{cases} a_2 \sin(\pi t/t_1) & (0, t_1) \\ -a_4 \ \sin(\frac{\pi t}{t_2} + \pi - \frac{\pi t_1}{t_2}) & (t_1, t_1 + t_2) \end{cases} \quad (37)$$

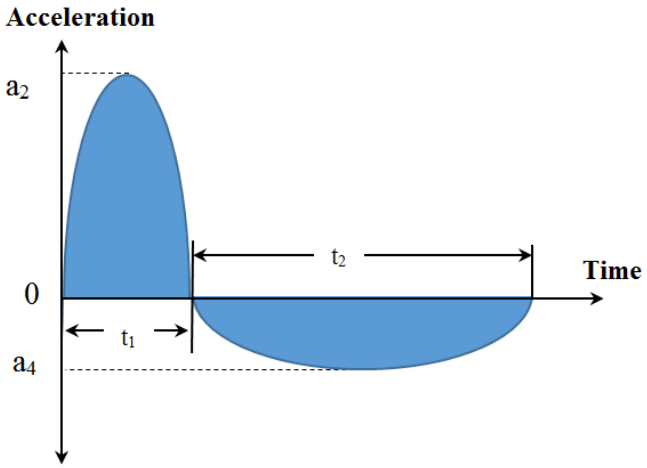

Figure 26 Impulse sinusoidal signal, available from (Emre Demír, 2015)

(Wang, Wang, & Chen, 2008) Present a way to estimate the peak acceleration value on the supporting spot that can be calculated using the following equation:

$$\mathrm{A}_e = \frac{2\, P_m\, A_s \cos\varphi}{\Delta} \quad (38)$$

Where A_s is the effective bearing area of the bilge, φ is the angel between the horizon and the external plane of bilge. Δ is the tonnage of the ship. P_m is maximum peak pressure on the spot of the bilge.

2.6. Shock design criteria for surface ships (DDAM).

(McCarthy Jr., 1995) NAVSEA refers as a reference manual to provide a shock design criteria for shock design calculations, and to deliver a general background concerning the application

of the Dynamic Design Analysis Method (DDAM). The DDAM are used by the American and British NAVY's.

This set of rules takes into account the DDAM and its predecessor G design method, to evaluate the shock capability of onboard equipment. The DDAM was designed in a period where access to computers was limited, and computer codes were simple. That is why the DDAM is a rapid and efficient method, often used at low time predesign stage.

The DDAM reduces the equipment or structure to an equivalent mass elastic system which is used to design the equipment's, with the objective to sustain the dynamic stresses induced by shock response motions. By setting up and solving the equations of motion of this mass-spring system, forces and displacements associated can be obtained.

The specified shock spectrum design acceleration for every kind of equipment are used as data for the DDAM. They are usually obtained from large scale tests as well as data recorded from the vessel operation. Once the shock spectrum design acceleration is known, the DDAM can be divided into 5 interconnected phases:

1. Problem formulation phase
2. Mathematical modeling
3. Coefficient computation phase
4. Dynamic computation phase
5. Evaluation phase

2.6.1. Problem formulation phase

This phase takes a look of the detail design of the structure in study. The analyst should determine the shock grade of the equipment or structure, the mounting location of the foundation, the shock design value to be used, and the critical areas of the system which may have specific modeling considerations.

2.6.1.1. Shock grading

- **Grade A**: are applicable to items which are required, for the performance or direct vital support of mission-essential functions onboard of shock hardened ships: The following are mission essential functions.

- **Grade B**: this is related to items whose operation are not essential to the safety of the ship, or present a direct and vital role during the mission-essential functions identified above but which, due to either location or function can represent hazard to personnel.

2.6.1.2. Mounting locations

All the equipment and structures can be hull mounted, deck mounted, or shell mounted as it can be observed in Figure 27.

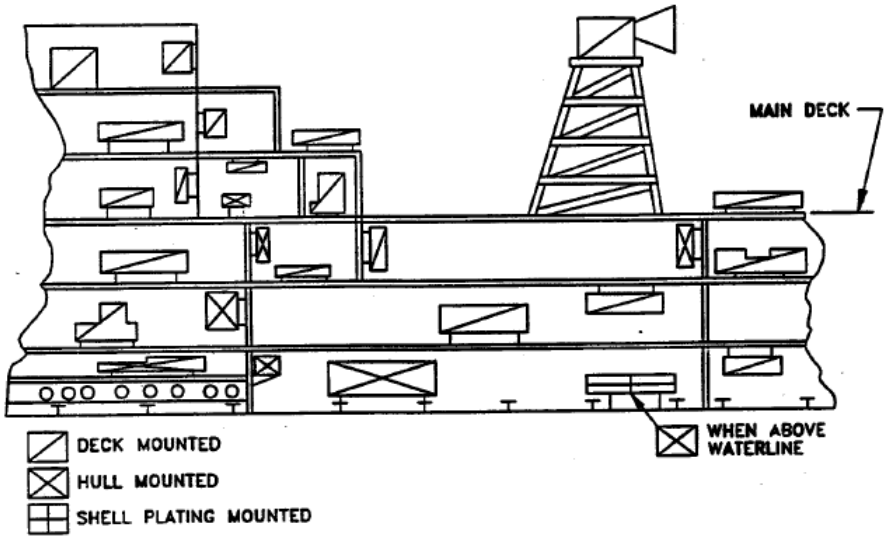

Figure 27. Different mounting configurations for embarked materials. Available from: (McCarthy Jr., 1995)

- ***Hull mounted***

This refers to the equipment mounted, on basic hull framing, such as tank tops, inner bottom, shell plating above the water-line and structural bulkheads below the main deck (bulkhead deck). Where a structural bulkhead (Grounded at the inner bottom) contacts the main deck, deck below main deck, shall be considered as hull mounted.

- ***Deck mounted***

Shock design values are used for equipment mounted on decks, platforms, non-structural bulkheads, and structural bulkheads, above the main deck..

- ***Shell mounted***

This corresponds to equipment directly attached to the shell plating below the waterline. When two equal pieces of equipment are attached to the ship, the larger shock design value should be adopted.

2.6.1.3. Shock design values

a. Elastic shock design values

These values should be used, when it is necessary to preserve the original physical dimensions after exposure of the shock, especially where high precision clearances are needed such as propeller shafting. Foundations for rotating auxiliary equipment should be designed, elastically; proving that plastic deformation or tilting of the mounting surface will not occur, or will not impaired the ship performance. Proper selection of shock design values should be considered by the designer and the contractor.

b. Elastic-Plastic Shock design values

It is used in cases where design by dynamic analysis is required.

c. Special criteria for displacement-critical items

This is critical design where deflections are critical from a shock standpoint. These calculations shall be based upon elastic design values.

d. Special criteria for Hold-Down/ Locating Devices:

In cases where foundations are designed to suit elastic-plastic, velocity limited shock design values should be developed by the use of the elastic shock values, for the analysis of bolting dowels, and similar hold down locating devices. This analysis should be performed to devices attached to the shipboard foundation. Hold-Down locating devices which are not at the

foundation of the equipment shall follow the design criteria that apply to other structural elements of the equipment.

2.6.2. Mathematical modelling phase

This phase consists in the representation of the significant dynamical characteristics of the system under consideration, by means of masses and structural elements such as beams springs and plates.

A separate analysis should be considered for each principal direction of shock loading, and should be evaluated separately. For a Multi Directional Response (MDR), a single mathematical model may be enough for the three directions of input. The mathematical modeling phase passes through the following steps:

1) Basic modeling assumptions
2) Frequency calculations
3) Mass lumping
4) Mass locations
5) Designation of structural model
6) Special modeling criteria

2.6.2.1. Basic modeling assumptions

One of the fundamental assumptions necessary for the application of DDAM is the selection of a fixed base. A fixed base acts as rigid stationary boundary in the direction of the shock, transmitting the shock motion to the mounted equipment or structure. The fixed base is assumed to be the interface between the system foundation and the ship structure. Proper selection of the fixed base, whether it is hull or deck mounted, will also define the proper selection of the shock design values. It is necessary for the model to reflect the flexibilities of the interface which can affect the system response.

2.6.2.2. Frequency calculations

Fixed base natural frequency calculations are used to determine those components which are critical. These components may require a separate mass or masses to properly model them. The cut-off frequency is defined as the highest mode of vibration to be considered by the conditions specified. The components of the model which are below the cut-off frequency shall be modeled.

2.6.2.3. Mass lumping

Once the critical areas are identified; the modeling of the problem should be done taking into consideration the following points:

a) Model simplicity: The model should be as simple as possible, without omitting important information.

b) High frequency components should be lumped together: high frequency components with adjacent frequencies will need to be merged together.

c) Low frequency elements should be modeled as separated masses.

d) Shock test items shall not be included in the model. The rules focus on the analysis only on representative systems.

2.6.2.4. Mass locations

The masses of the representative equipment should be in relation with the fixed origin. The proper system of coordinates should be used, in relation to the fixed frame of reference.

2.6.2.5. Designation of structural model

The structural model which is linear, elastic, having a mathematical description, can also be represented by a finite element model. The structural model, describes the item in terms of physical characteristics, which when combined with concentrated masses will produce a dynamic characteristics representative of the equipment, or system.

2.6.2.6. Special modeling criteria

During the coefficient computation phase and dynamic computation phase, all the resilient mounting characteristics shall be taken into consideration for the mathematical modeling. For equipment that has piping connections, which is not separated from the model, the analyst shall include the weight, up to five feet of piping, including its content as mass when modeling the equipment.

At the locations, where foundations are grounded on deep frames, such inner bottom structure, built-in tanks, or similar structure above, this structural flexibility should be taken into account. The incorporation, of this flexibility may lead to a reduced shock response calculation.

2.6.3. Coefficient Computation Phase

In order to obtain the reaction of the model to a shock, it is then necessary to solve the motion equation:

$$[M]\{\ddot{X}\} + [C]\{\dot{X}\} + [K]\{X\} = \{P(t)\} \quad (39)$$

Where $X, \dot{X}, \ddot{X}$ = are displacement, velocity and acceleration respectively, of a nodal degree of freedom and $P(t)$ is the externally applied force function. $[M]$ is the mass matrix and [C]is the damping matrix, which is not considered by the DDAM.

The mass matrix coefficients $[M]$ can be determined by the lump mass, or the consistent mass formulation. The simplest procedure to define the lumped mass properties, of any structure consists in assuming that the distributed masses are located at the nodes, where the translational displacements are defined, and all the magnitude of the mass is located at each node.

2.6.4. Dynamic computation phase

In this phase, it is necessary to carry out the modal analysis of the system being analyzed. In this matter there are many computer programs available to obtain the modal characteristics of the analyzed system.

2.6.4.1. Modal Analysis

The mathematical model representation of a system or structure, involves the definition of a modal (frequency) equations of motion for that system. For an un-damped free-vibrations; the modal equations, for a multi-degree of freedom system, the matrix modal equation system writes:

$$-w^2[M]\{\phi\}_a + [K]\{\phi\}_a = \{0\} \quad (40)$$

The solution of this matrix system allows to obtain the natural frequencies w_a and mode shapes$\{\phi\}_a$.

2.6.4.2. Dynamic reduction techniques

Large amounts of degrees of freedoms can create significant issues due to its large complexity. Although there are some risks regarding the conversion of complicated models to more simplified models, matrix reduction techniques, such as kinematic condensation: Kynematic Condensation (Guyan Reduction), Generalized Dynamic Reduction (Rayleigh-Ritz) and Component Mode Synthesis (Sub-structuring).

2.6.5. Evaluation Phase

During this phase, the levels of deflections in the equipment, structure and/or foundation are analyzed and compared to specified failure criteria, established according to operational considerations. A static analysis is performed within each mode the system is in equilibrium. The phases included in this phase are:

- Modal assessment.
- Shock design values to apply.

- Number of modes to use.
- Combining stresses within each mode.
- Summing stresses across the modes.
- Combining operating and shock stresses.
- Response assessment.

2.6.5.1. Modal assessment

The modal analysis of the system generates dynamic response characteristics (frequency and mode shapes) which should be reviewed with care, verifying that requirements of the DDAM are satisfied:

- Very low frequency of the composing systems (less than 5 Hz).
- Closely spaced modes.

Critical closely spaced modes may occur with modes having large modal masses, and are the ones which are separated within a gap of 10% of the common mean frequency. To identify properly these modes, it is very convenient to create a graph of modal effective mass versus modal frequency; this will help to identify potentially hazardous modes, which are usually two or more modes close in frequency having considerable magnitude with the rest of the spectrum.

2.6.5.2. Number of modes to consider

The number of modes to be calculated needs to be sufficient to satisfy the modal weight requirement, which should not be less than 80% of the total weight of the system. Modes considered affecting critical parts of the equipment shall also be considered. Other modes to be included are the ones which the nodal acceleration exceed the 10% of the maximal.

2.6.5.3. Calculating stresses within each mode

The following stress formula shall be used in each mode to calculate the maximum modal stress: The NRL summation procedure, outlined in next § 2.6.5.4, is then applied to obtain a total shock stress summed across the modes. The Von Mises Theory of failure is used to determine the

modal stress σ_a in a structural member subjected to both normal and shear stresses. The formulas to be used are as follows:

For the uni-directional case, the modal stress σ_a for the ath mode is given by:

$$\sigma_a = \sqrt{\sigma_{nom}^2 + 3\,\tau_{Shear}^2} \tag{41}$$

Where, σ_{nom} is the normal stress τ_{nom} is the shear stress. For two and three dimensional stress state analyses respectively:

$$\sigma_a = \sqrt{\sigma_x^2 - \sigma_x\,\sigma_y + \sigma_y^2 + 3\,\tau_{xy}^2} \tag{42}$$

$$\sigma_a = \sqrt{\sigma_x^2 + \sigma_y^2 + \sigma_z^2 - \sigma_x\,\sigma_y - \sigma_y\sigma_z - \sigma_x\sigma_z + 3(\tau_{xy}^2 + \tau_{yz}^2 + \tau_{xz}^2)} \tag{43}$$

Where:

σ_a: is the stress state associated to the mode number a.

σ_x , σ_y , σ_z : are the normal stresses along the X,Y and Z directions.

τ_{xy} , τ_{xy} , τ_{xy}: represent the shear stresses.

2.6.5.4. Summing stresses across the modes

A basic method to determine the acceptability of the design is proposed by NRL and consists in combining the responses over the modes. To calculate the total shock stress or the total relative deflections, the NRL uses the following formula:

$$R_i = |R_{ia}| + \sqrt{\left(\sum_{b=1}^{N} R_{ib}^2\right) - R_{ia}^2} \tag{44}$$

R_{ia}: is the largest modal stress or deflection (for all of the modes selected) at the point *i*

R_{ib} : represents each member of the complete set of stress or deflection contributions at point *i*

2.6.5.5. Combining operating and shock stresses

To compare the stresses produced by the shock loading with specified failure criteria, the Von Misses operating stresses coming from a shock dynamic analysis need to be sum with the operating stresses, such as the stresses coming from the shock dynamic analysis need to be sum to the operating stresses, such as the stresses present in rotating element:

$$\sigma_{total} = |\sigma_{shock}| + |\sigma_{oper}| \tag{45}$$

2.6.5.6. Response assessment

For the cases that the stresses obtained exceed the given criteria, a further analysis should be performed in other to determine if the level of the responses can be reduced to a permissible level.

Redesign or remodel: If the high Reponses are not caused by closely spaced modes; the items shall be redesigned to have stresses within acceptable limits.

The closely spaced method (CSM): this is method used to combine one or more closely spaced modes into one mode. This method is restricted to mode pairs which have frequencies within 10% of the common mean frequency, and have amplitudes which are opposite in sign.

The algebraic summation method (ASM): this is an alternate method which combines modal responses that preserve the phase relationships among the modes.

Using the CSM and ASM will produce more credible results if closely spaced modes are the identified to be the cause of the high calculated responses.

3. ELASTOPLASTIC REPSONSE ANALAYSIS OF A SHIP SECTION SUBMITTED TO A SHOCK WAVE.

3.1. Introduction

The integrity (non-destruction) of the hull of a given ship submitted to the shock wave produced by an UNDEX is usually restricted to the analysis of one hull stiffened panel bounded by two decks and two bulkheads.

As it is mentioned by (Barras, 2007), theoretical approximations can be used to evaluate the integrity of the plating that is facing the shock wave profile.

During the intership at STX Europe at the department of Vibration and Acoustics, a step by ste procedure was done in order give an approximation to analyze a ship section subjected to a shockwave. The procedure considers the use of two formulations usign blast wave approximations, one which calculates the initial speed for a plate when subjected to an underwater explosion, and second one which uses time history pressure profile applied to the plate. Both formulation were confronted with experimental data available in the literature, by the use of the finite element software LS-DYNA. The comparison obtained for the pressure time history an the experimental results show accordance.

In order to proportion a appropiate tool to STX to perform the analysis of an underwater explosion, the same set of simulations were used to verify that the results obtained using LS-DYNA were similar to ANSYS taking the appropiate considerations. Two additional models were constructed to verify the correspondance in results using LS-DYNA and ANSYS that is an stifffened pannel and finally the ship section were also performed showing the correspondance.

3.2. Planar wave approximation (PWA)

According to (Hollyer, 1959) one of the ways to characterize the damage caused by an UNDEX onto a ship consists in starting the analysis by studying unstiffened still plates. The modeling of an UNDEX using an infinite plate and a shock wave can be made with minimum assumptions. The simplified problem can be easily to get a rough but useful approximation.

The interaction between an infinite plate and a shock wave can happen in two scenarios, an air-backed or water-backed plate. The basic analysis consists in applying the continuity of flow principle. The striking incident shock wave of an air-backed plate occurring in a perpendicular direction, the incident velocity of the particles is made equal to the reflected water particles velocity plus the plate velocity.

$$\frac{P_i}{\rho c} = \frac{P_r}{\rho c} + v \quad or \quad P_r = P_i - \rho c v \tag{46}$$

The value P_i is the incident pressure; P_r is the reflected pressure, ρ is the water density, v is the speed of the plate and c is the speed velocity of sound in water. Knowing that the total amount of pressure acting on the plate is equal to $P_i + P_r$ and applying the equation (46) **Erreur ! Source du renvoi introuvable.** the total pressure P_t acting on a plate can be described as:

$$P_t = 2P_i - \rho c v \tag{47}$$

If the restoring forces are not considered, the equation of the system can be expressed as:

$$\mathrm{m}\ \frac{\mathrm{dv}}{\mathrm{dt}} = 2\mathrm{P_i} - \rho \mathrm{cv} \tag{48}$$

As described at the equation 0 the pressure arriving at the standoff point P is:

$$P_i = P_o\, e^{-t/\theta} \tag{49}$$

The equation 0 can then be written as:

$$v = \frac{2P_o}{\rho c}\frac{1}{Z-1}\left(e^{-\frac{t}{Z\theta}} - e^{-\frac{t}{\theta}}\right) \tag{50}$$

In this case $z = m/\rho c\theta$ is a control function. The pressure acting in unit per area on to a plate is expressed by:

$$P = \frac{2P_o}{\rho c}\frac{1}{1-Z}\left(Ze^{-\frac{t}{\theta}} - e^{-\frac{t}{Z\theta}}\right) \tag{51}$$

Equation (51) shows that the pressure may vanish; producing cavitation at the interface between the plate and the fluid (the plate then separates from the fluid).

3.3. Spherical wave approximation (SWA)

The spherical wave approximation as referred in (Barras, 2007) consists in assuming that the shock wave received by a submerged flat plate presents a spherical profile, based on the condition that the charge is located quite near the plate, as it is shown in Figure 28.

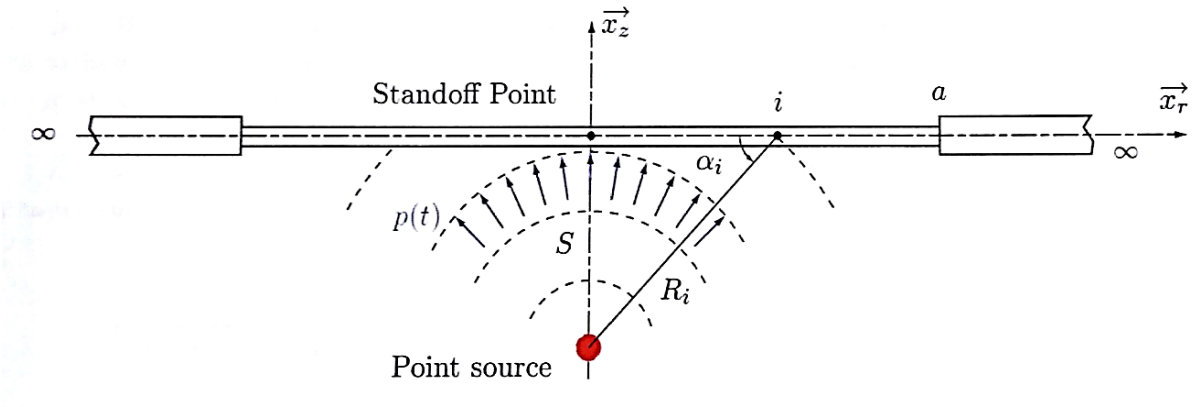

Figure 28. Spherical wave approximation. Available from (Barras, 2007).

The conservation of momentum writes:

$$m_i\frac{dv_i}{dt} = 2p_{Ii}(t) - \frac{\rho c v_i(t)}{\sin\alpha_i} \tag{52}$$

That can similarly be expressed as:

$$\frac{dv_i}{dt} + \frac{\rho c}{m_i \sin\alpha_i}v_i(t) = \frac{2p_m}{m_i}\frac{S}{R_i}e^{-(t-\tau_i)/\theta} \tag{53}$$

Assuming that the plate is uniformly thick, a non-dimensional coefficient can be introduced:

$$\beta_i = \frac{\rho c \theta}{m \sin \alpha_i} = \frac{\beta}{\sin \alpha_i} \tag{54}$$

In this case, β_i represents the mass unit displaced by the shock wave in the normal direction of the plate, and $\tau_i = (R_i - S)/c$ is the delay of the shock wave to reach the point i. Assuming that this time is negligible, the general solution of the equation for the speed at a point i can be written as:

$$v_i(t) = \frac{2 \sin \alpha_i \, p_m}{m} \frac{\theta}{(1 - \beta_i)} \left(e^{-\beta_i t/\theta} - e^{-t/\theta} \right) \tag{55}$$

To find the maximum speed profile, it is necessary to equal the derivate from the (Eq. (58)) to cero and obtain the time at which the maximum peaks occurs, which is:

$$t = \theta \left(\frac{\ln \beta_i}{\beta_i - 1} \right) \tag{56}$$

Solving (Eq. (55)) at the time given by (Eq. (56)) the speed of a particular point can then be represented by:

$$v_{im} = \frac{2 \sin^2 \alpha_i \, p_m}{\rho c} \, \beta_i^{\,1/(1 - \sin \alpha_i)} \tag{57}$$

3.4. Impulse response analysis of a circulate plate

In order to verify the applicability of the approximations that were mentioned above, finite element simulations of a circular plate submitted to spherical wave pressure loads have been carried out and the resulting plate deflections have been compared to some results extracted from (Barras, 2007), who used the more sophisticated code LS-DYNA-USA, taking into account all the effects of fluid structure interactions. Table 2 shows the geometrical dimensions of the model, as well as the propperties of the material used.

Table 2. General parameters of the circular plate.

Plate radious (m)	0.2664
Thickness (mm)	2.79

Density (Kg. m^-3)	7800
Yield strength (N.m^-2)	240 x10^6

Table 3. Parameters used in the underwater explosion.

Fluid density (Kg. m^-3)	1025
Sound speed (m.s^-1)	1500
Explosive mass(kg)	0.45
Stand-off distance(m)	1.827
Peak pressure (N.m^2)	18.7325 x 10^6
Time constant (ms)	0.0807953

The plate is modeled using Belytchko-Lin-Tsai shell elements and only 1/4th of the plate is modeled, taking advantage of the symmetry conditions of the plate. (Figure 29) shows the representation of the 3D model developed in LS-DYNA

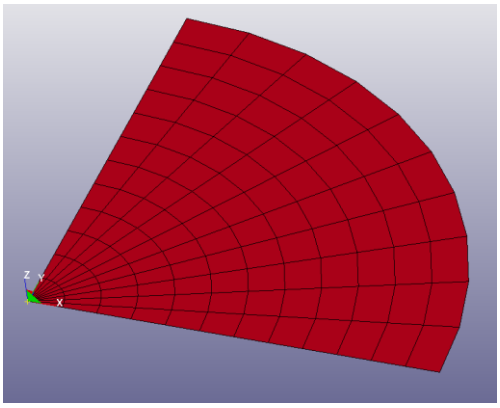

Figure 29. 3D Plate shell element model.

It is important to mention that the model incorporates the symmetry conditions given at the x and y axis. Boundary conditions along the y axis are:

$$r_z = r_x = u_y = 0 \tag{58}$$

and boundary conditions along the x axis write:

$$r_z = r_y = u_x = 0 \tag{59}$$

Finally the boundary condition used at the border of the plate

$$u_x = u_y = u_z = 0 \tag{60}$$

The impulse velocity field such as defined by Eq.57 is applied to the nodes of circular plate model, using *INITIAL_VELOCITY_NODE LS-DYNA card. A Scilab code has been built in

order to calculate the velocity values from the parameters given in Table 3 and to apply the correct value to the correct node; taking into account the delay of arrival of the shock wave at each node. An example of resulting field is shown in Figure 30.

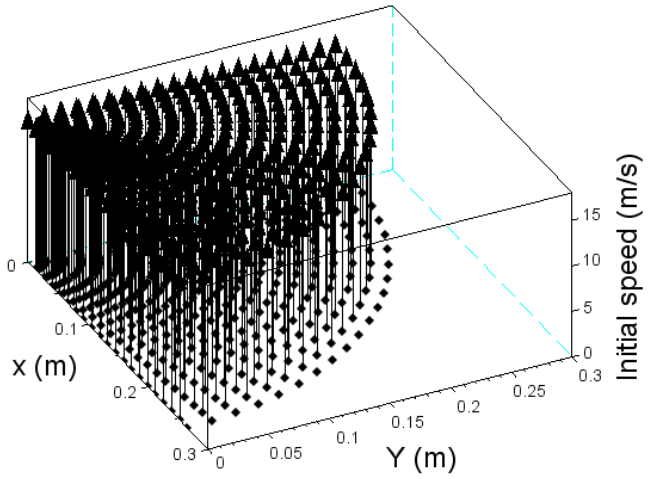

Figure 30. The initial speed vector profile applied to the plate.

Figure 31 graph compares the plate central node deflection obtained from our impulse velocity LS-DYNA simulation to the deflection calculated by (Barras, 2007) using the package LS-DYNA/ USA. It appears that the initial impulse approach underestimates the plate deflection, which is explained by the fact that, contrary to LS-DYNA/USA, the "Long time" water inertia effects are not considered by this approach.

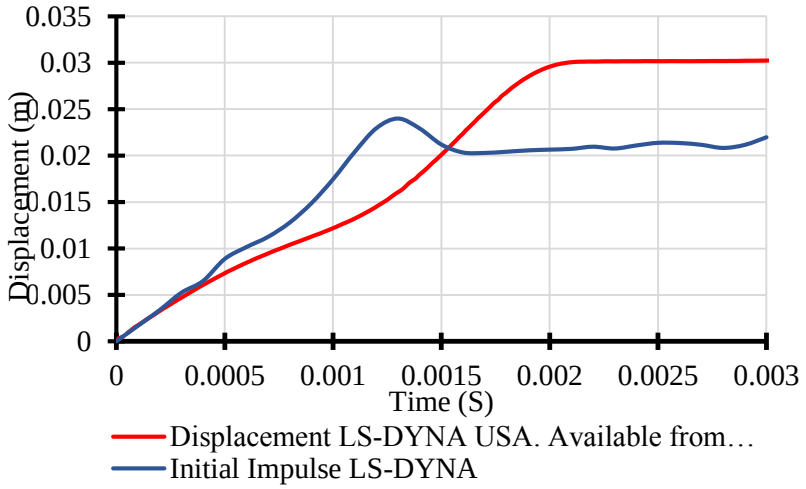

Figure 31. Displacement response from the central node of the plate.

Figure 32 compares the central node speeds. At the initial portion of the function it can be seen that the initial speed of both codes present about the same initial speed value, at the central node. The oscillations characterizing the impulse velocity response are due to the lack of water damping, (which appears in the reality).

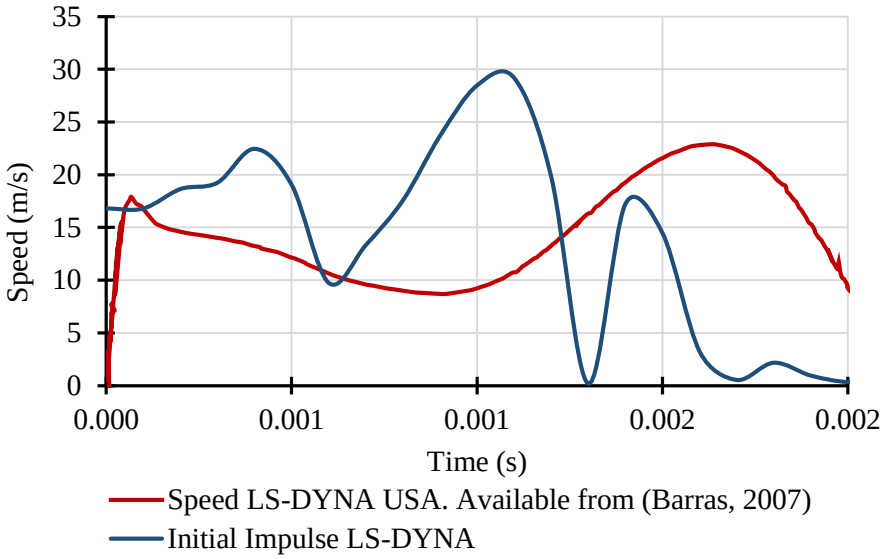

Figure 32. Speed response from the central node of the plate.

3.5. Impulse response analysis of a rectangular plate

In order to appreciate the validity of the initial impulse velocity approach, additional simulations were performed and compared to real experimental results performed by (Ramajeyathilagam, K.; Vendhan, C.P.; Bhujanga Rao, V., 2000) as well as the results obtained from their modeling using a pressure history applied to a plate. This set of experiments were performed using high strength steel and mild steel. The total size of the plate used was 0.55 x 0.45 m^2 with an exposed area of 0.30 x 0.25 m^2 and a thickness of 4 mm. The corresponding material characteristics can be seen in following Table 4.

Table 4. High strength and mild steel properties.

HS steel		Units
Elastic modulus	2,1 x 10^5	MPa
Poisson's ratio	0,3	
Mass density	7800	Kg/m^3
Tangent Modulus	250	MPa
Static yield stress	400	MPa

MS steel		Units
Elastic modulus	2,1 x 10^5	MPa
Poisson's ratio	0,3	
Mass density	7800	Kg/m^3
Tangent Modulus	250	MPa
Static yield stress	250	MPa

Rupture Strain	0,23	

Rupture Strain	0,18	

Since the underwater explosion is a very rapid event and the loads applied to the structure are very rapid, the influence of the strain rate of the material dynamic behavior must be taken into consideration. Usually the effect of the strain rate is modeled by using the Cowper Symonds law, defined by the following equation:

$$\sigma_{dy} = \sigma_y \left(1 + \left|\frac{\dot{\varepsilon}}{D}\right|^{1/n}\right) \quad (61)$$

Where σ_{dy} is the dynamic yield stress, σ_y is the static yield stress, $\dot{\varepsilon}$ is the strain rate, *D* and *n* are coefficients obtained from experimental measurements and curve fitting procedures. These coefficients are largely referenced in the bibliography for both high strength steel and mild steel: D = 40 s^{-1} and n = 5.

Figure 33 shows how the symmetry of the plate is considered by Ramajeyathilagam et al. for the modeling.

Figure 34 shows finite element model used in the simulation, again taking advantage of the symmetry conditions, and using a mesh of 30 x 30 elements, instead of the 5 x 5 elements presented in the article to proportion extra accuracy. Fully clamped boundary conditions are applied at the outside borders of the plate and the symmetry conditions are modeled as follows:

- along the y axis: $u_x = 0 \quad r_z = r_y = 0$ (62)

Along x axis:

-along the x axis: $u_y = 0 \quad r_z = r_x = 0$ (63)

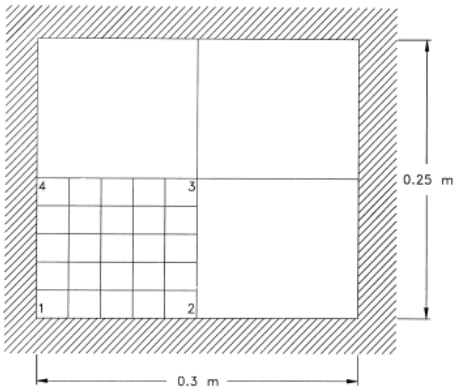

Figure 33. Finite element modelling of the plate. Available from (Ramajeyathilagam, K.; Vendhan, C.P.; Bhujanga Rao, V., 2000).

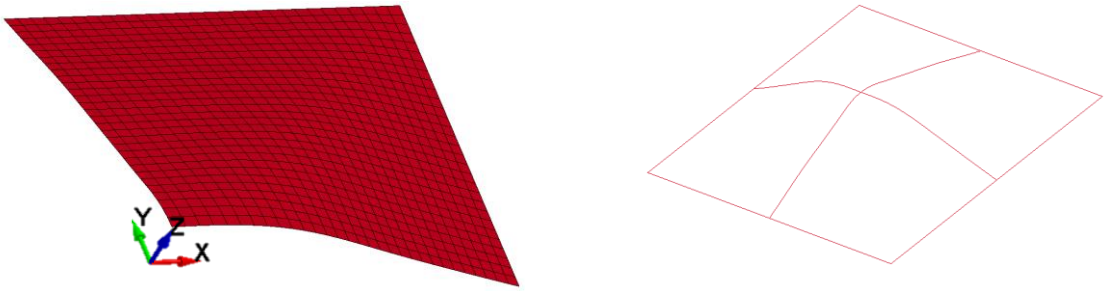

Figure 34. Quarter plate modelling using LS-DYNA.

The article presents 15 experimental measured results compared with simulations with and without accounting for the strain rate effect. Permanent deformation at the center of the plate is given for 10 of these experiments. Table 5 shows the parameters used in each one of the experiments and the corresponding results.

Table 5. Parameters given for the different experiments. Available from (Ramajeyathilagam, K.; Vendhan, C.P.; Bhujanga Rao, V., 2000).

No	Experiment	Charge weight in (g)	Standoff distance (m)	Shock Factor	Total peak pressure in (MPa)	Permanent deformation (m)	Remarks
1	HS1	5	2	0,016	6,87	-	Elastic
2	HS2	5	1,75	0,018	7,99	-	Elastic
3	HS3	5	1,25	0,026	11,7	-	Elastic
4	HS4	5	1	0,032	15,04	-	Elastic
5	HS5	5	0,75	0,042	20,81	-	Elastic
6	HS6	5	0,5	0,064	32,9	0,003	Mode I
7	HS7	5	0,15	0,212	127,1	0,012	Mode I
8	HS8	10	0,15	0,3	165	0,023	Mode I

9	HS9	20	0,15	0,424	202	0,032	Mode I
10	HS10	50	0,15	0,671	302,6	0,059	Mode I
11	HS11	70	0,15	0,794	343,5	0,072	Mode I
12	MS1	50	0,15	0,671	302,6	0,0675	Mode I
13	MS2	60	0,15	0,735	324,1	0,0721	Mode I
14	MS3	70	0,15	0,794	343,5	0,0759	Mode II
15	MS4	80	0,15	0,849	361,2	0,0915	Mode II

The modeling of the rectangular plate using LS-DYNA was also performed using the conditions presented in the article.

Initially, one of the eight experiments was used to compare the results obtained by LS-DYNA using the initial speed approach. Figure 35 shows the results comparison between initial speed approach and the pressure based input presented in the article using high strength steel. The results show the effect on considering and not considering the strain rate by the Cowper Symonds material model.

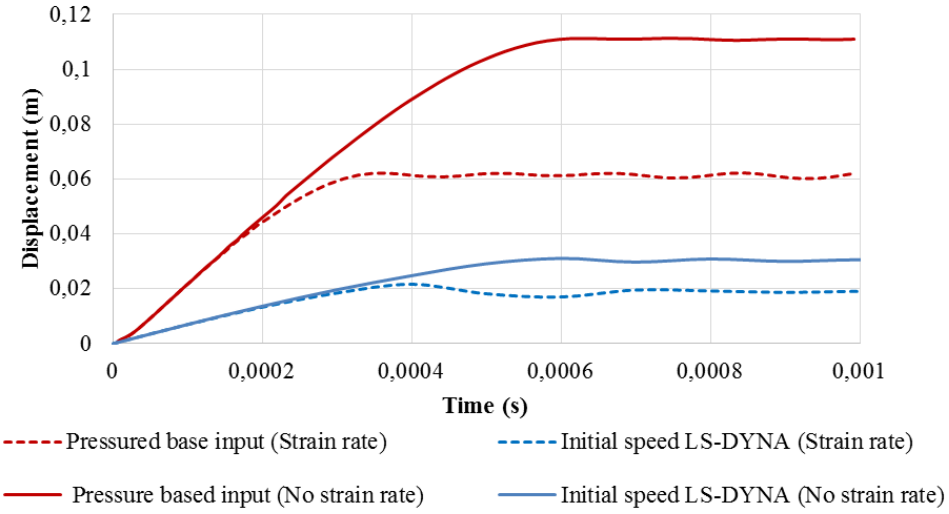

Figure 35. Central node displacement results for high strength steel and shock factor of 0.424.

As it can be seen from the previous results, the deflection of the plate central node is once again largely underestimated by the impulse velocity approach. Additionally, it is shown that the use of the strain rate effect on the modeling has serious attenuation effects on the obtained deflection levels.

Another analysis was performed using the same plate but another LS-DYNA functionality, *LOAD_SSA, which allows to account for both the primary shock wave and subsequent bubble oscillations loadings. The loading incorporates the plane wave approximation for the direct shock response and the virtual mass approximation for bubble response. As it it can be seen on the Figure 36, the plastic deflections obtained at the center of the plate do not differ sensitively, although the one calculated by LOAD_SSA functionality is a bit higher.

As shown by Figure 37 where velocity time histories have been plotted, the velocity peaks are found on the same values. Moreover, as the initial velocity assumption is concerned, it is stablished that at time cero the nodes of the plate receives an impulse that reaches almost the same speed after a certain time. In this last case, the time it takes to reach the maximum value will help to add more energy on the structure, causing a slightly higher deflection.

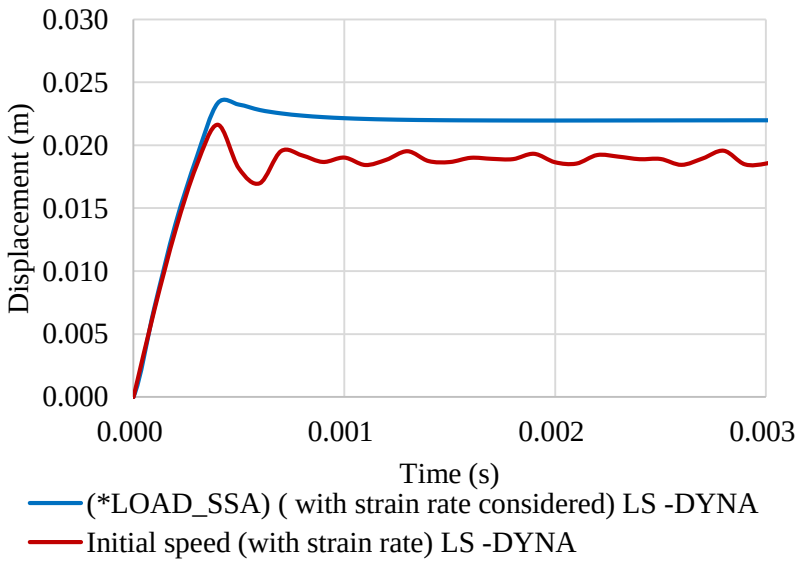

Figure 36. Displacement history of the central node of the plate, using the initial speed condition compared with the *LOAD_SSA input formulation.

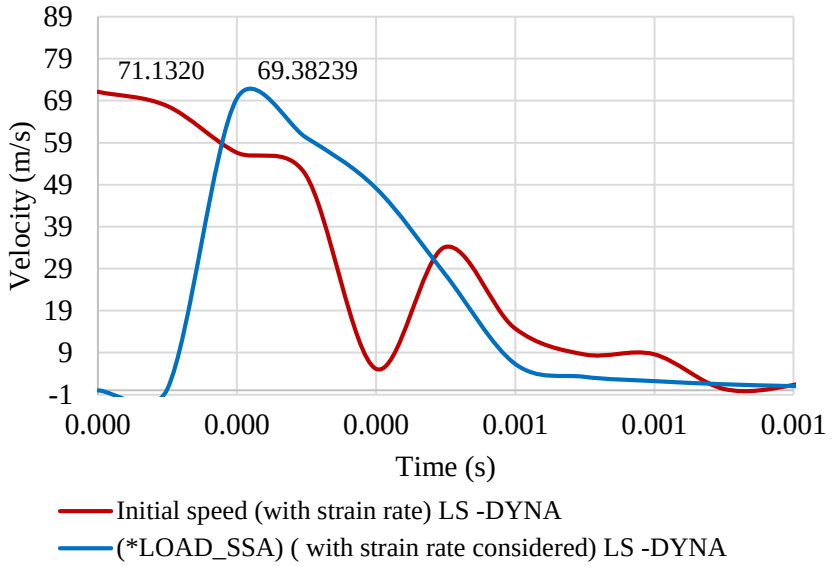

Figure 37. Velocity history of the central node of the plate, using the initial speed condition compared with the *LOAD_SSA input formulation

Finally, it can be stated that the spherical wave impulse velocity approach, as compared to the experiments or full LS-DYNA calculations leads to very underestimated and non-conservative results.

3.6. Spherical wave approximation using pressure

An additional way to assess the effect that a non-contact underwater explosion does to a structure is to calculate the time history of the pressure received by the structure and to apply it directly on the elements which compose the model. As it has been previously, the pressure which is received at point I (making angle α_i with the charge) by a plane structure impacted by spherical shock wave writes:

$$Pt_i = 2p_{Ii}(t) - \frac{\rho c v_i(t)}{\sin \alpha_i} \tag{64}$$

Where

$$2p_{Ii}(t) = 2P_o \sin \alpha_i \; e^{-(t-to)/\theta} \tag{65}$$

Remembering equation (55):

$$v_i(t) = \frac{2\sin\alpha_i\, p_0}{m}\,\frac{\theta}{(1-\beta_i)}\left(e^{-\beta_i t/\theta} - e^{-t/\theta}\right)$$

And also remembering that the non-dimensional coefficient is:

$$\beta_i = \frac{\rho c \theta}{m\sin\alpha_i} = \frac{\beta}{\sin\alpha_i}$$

At the end the equation that describes pressure input applied to each one of the elements is:

$$P_{element} = 2P_0\sin\alpha_i\, e^{-(t)/\theta} - \frac{\rho c\,\dfrac{2\sin\alpha_i\, Po}{m}\,\dfrac{\theta}{(1-\beta_i)}\left(e^{-\beta_i t/\theta} - e^{-t/\theta}\right)}{\sin\alpha_i} \qquad (66)$$

$P_{element}$ is the pressure applied to each of the shell elements on the plate and depend on the location of the charge, the angle as respect to the charge and eventually the arrival time of the shockwave (time delay effect) on each of the shell elements composing the plate as shown in

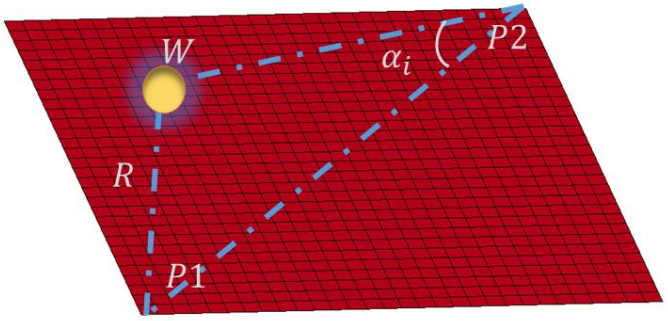

Figure 38. It also has to be mentioned that the second term of the previous equation is neglected to avoid having a pressure shortcut if the whole formulation is taken into account.

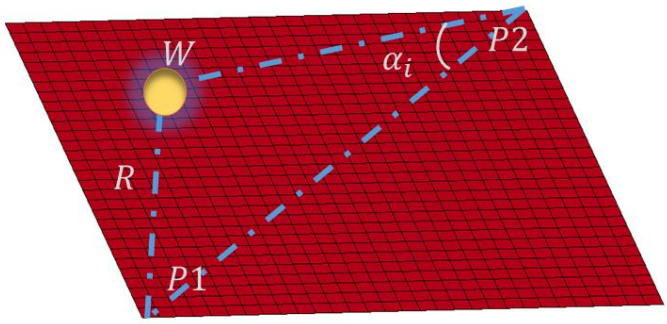

Figure 38. Quarter plate geometric representations for the SWA pressure based input.

Figure 39 shows the time history of the pressure which is applied to the plate furthest point *P2* and the closest one *P1* for a shock factor of 0.671 (same as in the article) for the plate as well as the incident free field pressure *Pi(t)*, associated to the underwater blast. The results of the free field curve and the *P1* can be compared with the data obtained in (Ramajeyathilagam, K.; Vendhan, C.P.; Bhujanga Rao, V., 2000).

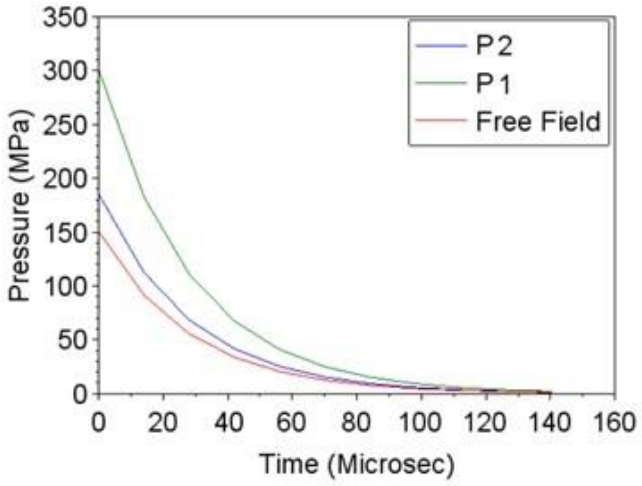

Figure 39. SF-0.671- Pressure time history at P1 and P2.

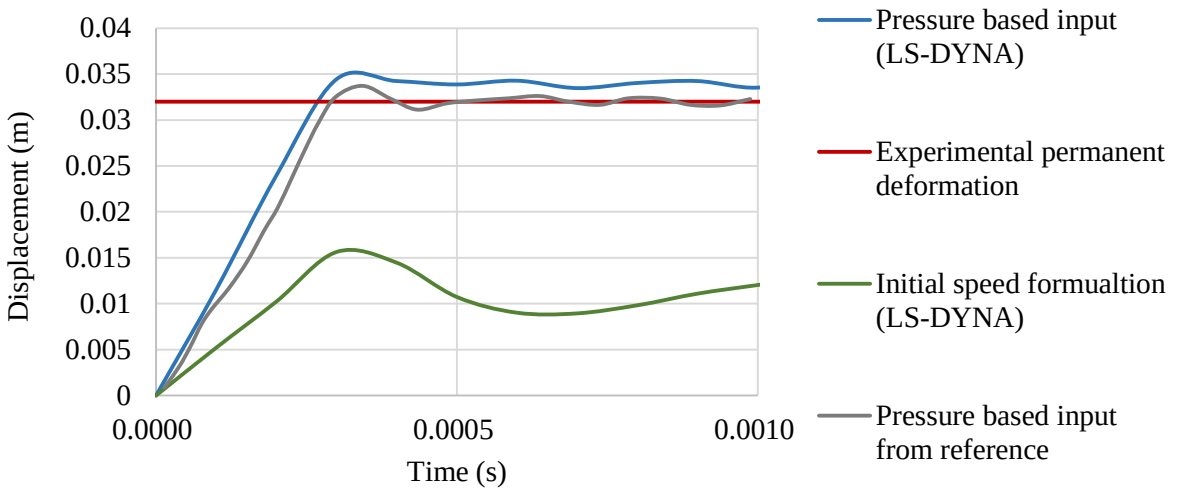

Figure 40 and Figure 41 compare plate center deflection time histories obtained by our pressure based approach (blue curve) to the experimental one (red curve), the impulse velocity one (green curve) and the pressure obtained by the authors finite element simulations, based on a planar wave based pressure approach seems to be conservative as it slightly over-estimates the measured final plastic deflection at the center of the plate. It is also worth noting that the discrepancy remains small (22.79% for mild steel and 7.19% for hard strength steel), considering that the formulation being used does not consider the effects of fluid structure interaction.

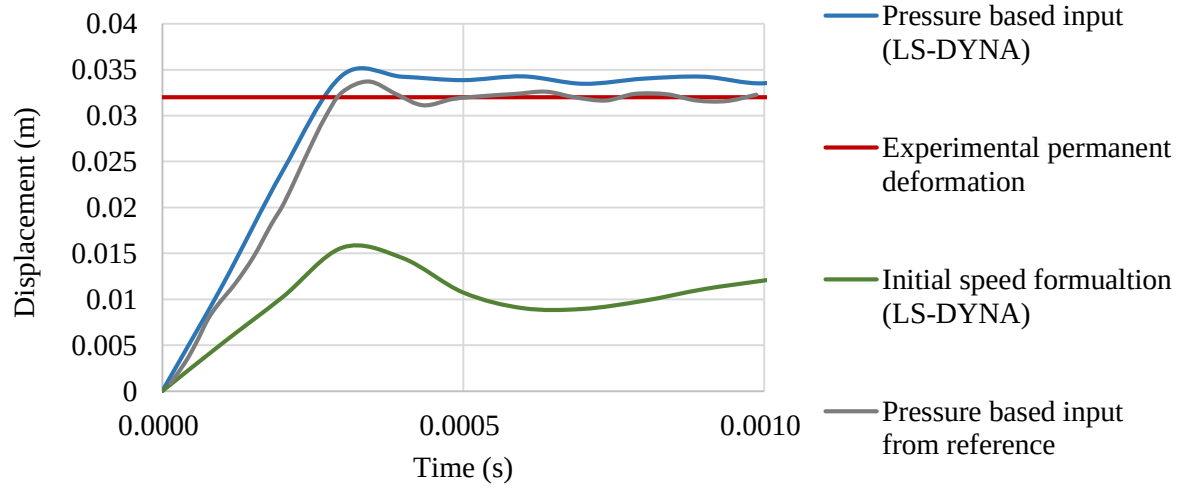

Figure 40. High strength steel. Shock factor 0.424.

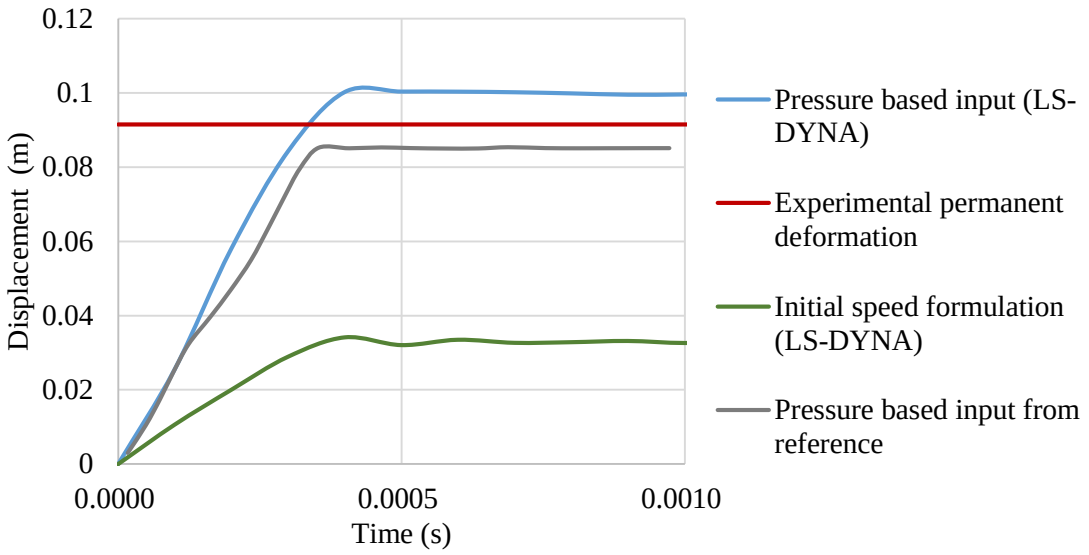

Figure 41. Mild steel. Shock factor 0.849.

Table 6 summarizes the six experimental results extracted from the mentioned article, compared with the results obtained from pressure based input from the SWA pressure based approach. For all of the considered shock factors, the pressure based approaches results bound the experimental ones while the impulse velocities approach, systematically underestimates the measured deflection.

Table 6. Simulation results comparison of the maximum deformation achieved.

Hard Strength Steel	Shock Factor (SF)	Experimental (m)	SWA Pressure based input (m)	%Error	Pressure based input (Article) (m)	%Error	Initial speed formulation (m)	%Error
	0,424	0,032	0,034	7,19	0,0337	5,38	0,0156	-51,25
	0,671	0,059	0,060	2,20	0,0550	-6,78	0,0228	-61,36
	0,794	0,072	0,074	2,78	0,0640	-11,18	0,0263	-63,47
Mild Steel	Shock Factor (SF)	Experimental (m)	SWA Pressure based input (m)	%Error	Pressure based input (Article) (m)	%Error	Initial speed formulation (m)	%Error
	0,671	0,0675	0,077	14,37	0,0678	0,44	0,0277	-58,96

	0,794	0,0759	0,093	22,79	0,0809	6,59	0,0322	-57,58
	0,849	0,0915	0,100	9,29	0,0854	-6,70	0,0341	-62,73

3.7. Time delay effect in the SWA pressure based input using LS-DYNA.

In the following tests, one of the cases of the plate is taken into account to show the effects of the time delay; the pressure input function is not applied until the wave reaches each of the elements which are used in the simulation. The following graph presents the time pressure history applied at different points on the plate, for the shock factor 0.424.

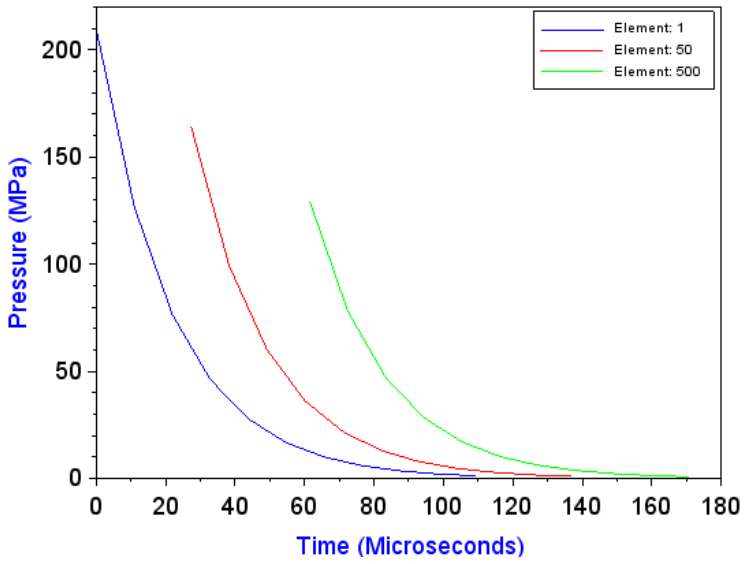

Figure 42. SWA pressure based input curves applied at different instants on the plate.

The model is based on the high strength steel structure and takes into account the strain rate effect of the material. This simulation is performed using LS-DYNA and just a quarter part of the plate is modelled, partially fixed at the borders (only rotations are allowed).

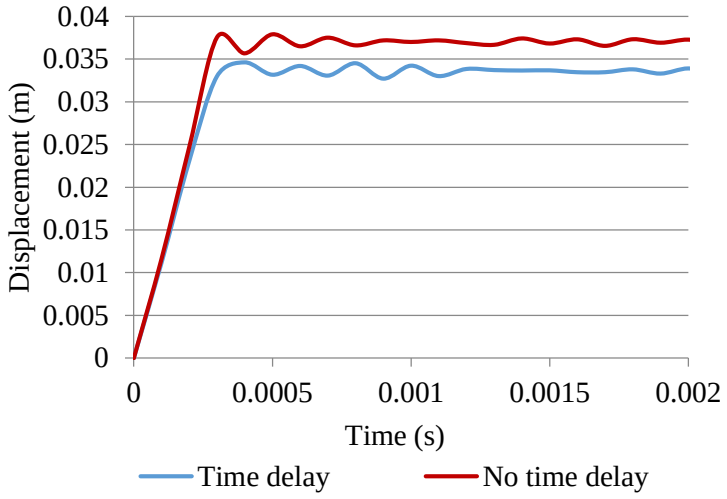

Figure 43. Attenuation of the central node displacement, due to the time delay effect. Shock factor of 0.424.

3.8. Comparison and validation using ANSYS & LS-DYNA

For the dynamic dimensioning of its structures, STX France uses the ANSYS general finite element software, based on an implicit time integration solver, while the explicit integration solver LS-DYNA is used in ICAM; it was necessary to prove that the results obtained using LS-DYNA are similar to those obtained with ANSYS. To do this, the same plate and the same input parameters as those presented in the previous section were used for simulations.

It is worth to mention here that for the simulations carried out with ANSYS, the transient solver needs to be activated, the time step needs to be defined as small enough to converge to one solution and the nonlinear effects such as plasticity and large displacements should be activated. It was also necessary to define in ANSYS a behaviour law that can take into account the strain rate effect of the material. ANSYS proposes the PERZYNA model, defined by the following expression:

$$\hat{\varepsilon}_{pl} = \gamma \left(\frac{\sigma}{\sigma_o} - 1 \right)^{1/m} \tag{67}$$

The material model proposed in ANSYS is similar to the equation Cowper Symonds law. It is thus necessary to define the corresponding behaviour law constants from Cowper Symond coefficient: 1/p = m and γ = D. The behavior law of the material can be seen in the Figure 44.

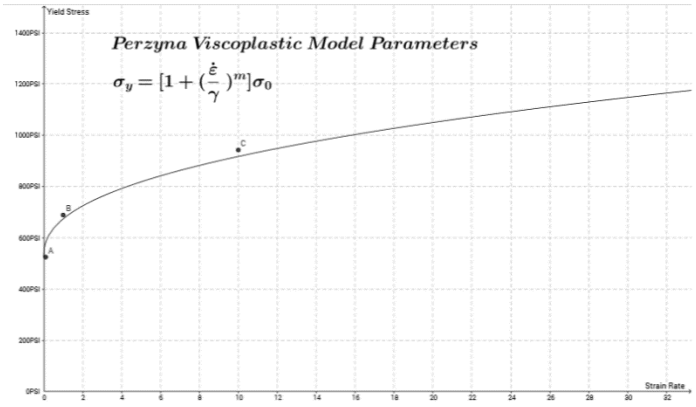

Figure 44. Perzyna viscoelastic law behaviour. Available from: https://www.geogebra.org/m/26707[Accessed 23 December].

In the formulation implemented in ANSYS, the time delay of the shockwave is not taken into account. Instead, the whole pressure time history for each of the composing SHELL181 element is applied at the same time. Figures 45 and 46 show the comparison of two tests using high steel and mild steel structures with shock factors of 0.424 and 0.849.

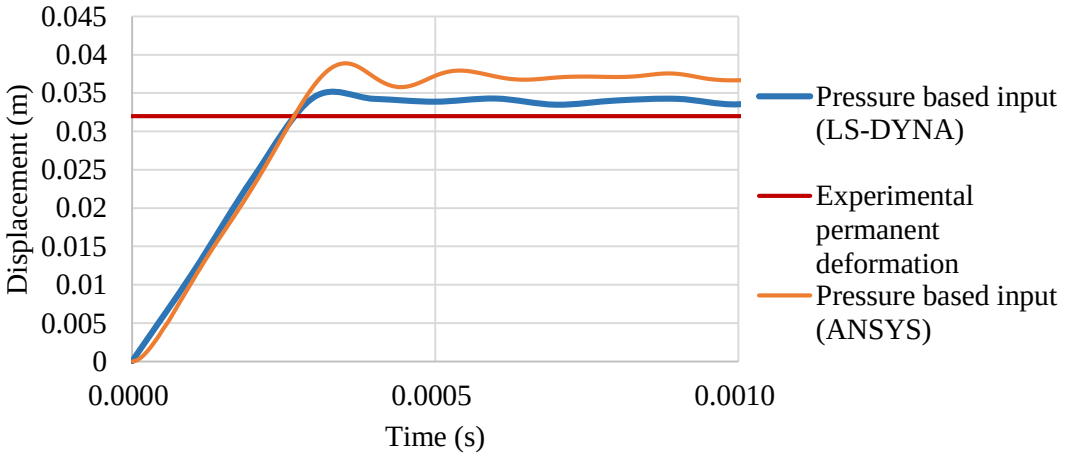

Figure 45. ANSYS LS-DYNA comparison results for high strength steel SF 0.424.

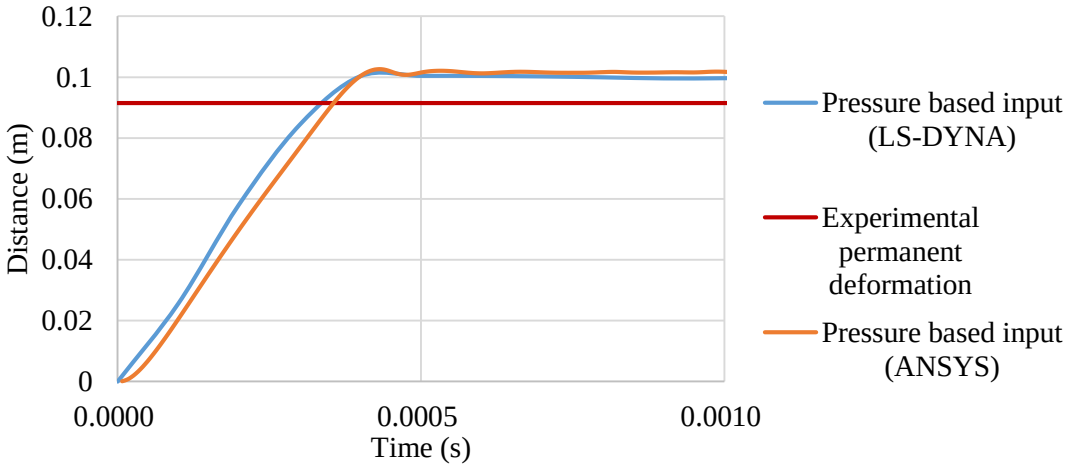

Figure 46. ANSYS- LS-DYNA comparison results for mild steel SF 0.849.

It can be seen from the pictures above that the deflection obtained numerically slightly exceeds the experiment deflection. The histories of the central nodal displacement for the six simulations are presented in appendix.

Table 7. Comparison results SWA ANSYS - LS-DYNA.

Hard Strength Steel	Shock Factor (SF) (m)	Experimental (m)	SWA Pressure based input (m) (LS-DYNA)	%Error	SWA Pressure based input (m) (ANSYS)	%Error
	0,424	0,032	0,034	7,19	0,0389	21,56
	0,671	0,059	0,060	2,20	0,0640	8,47
	0,794	0,072	0,074	2,78	0,0818	13,61
Mild Steel	Shock Factor (SF)	Experimental (m)	SWA Pressure based input (m) (LS-DYNA)	%Error	SWA Pressure based input (m) (ANSYS)	%Error
	0,671	0,0675	0,077	14,37	0,0814	20,59
	0,794	0,0759	0,093	22,79	0,0993	30,83
	0,849	0,0915	0,100	9,29	0,1030	12,57

In all the experiments showed on the Table 7, there is an overshoot on the results obtained using ANSYS as compared with the results using LS-DYNA. These discrepancies are due to the differences in the type of simulation as well as the possible differences on the material behaviour laws. It can also be stated that the results obtained using ANSYS are rather conservative.

3.9. Simple stiffened plate UNDEX analysis

New numerical finite element analyses were performed using LS-DYNA and ANSYS codes, accounting for the correct tangent modulus of the different tested materials. In other words, correct curves giving the real stress (Cauchy stress) as a function of the logarithmic strain were defined in ANSYS and LS-DYNA data files.

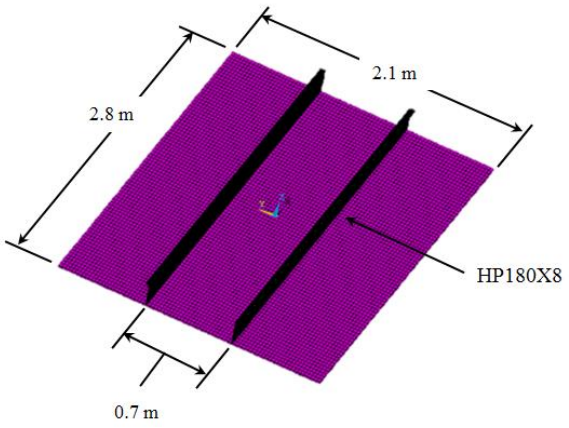

Figure 47. Finite element model used in the plate.

For these simulations, the charge is supposed to be located at a distance of 11.86 m and numerical simulations are run increasing progressively the charge weight until the maximum bearable shock factor without rupture of the plate is found. Only a quarter section a the full stiffened plate is modeled using shell elements and symmetry boundary conditions are applied such as shown by Figure 48.

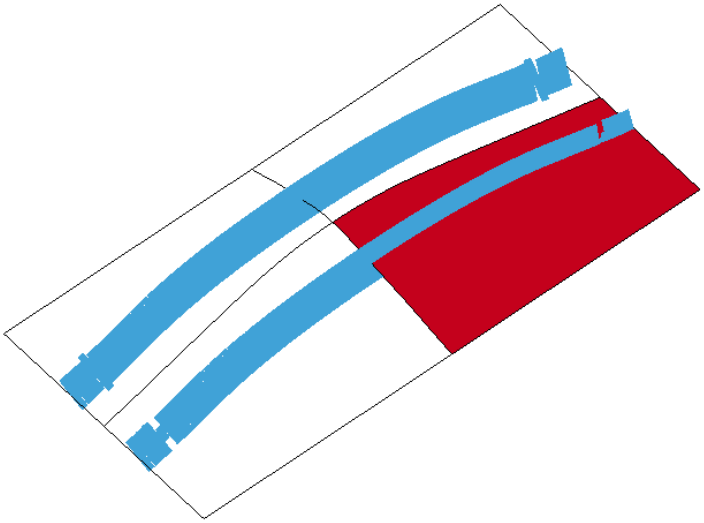

Figure 48. Symmetric boundary conditions applied to the model.

The failure strain thresholds value associated to the steel elastoplastic erosive law is calculated from a formula given by Lehmann, which takes into account the thickness *t* of the plate and the average length l_e of the shell finite elements:

$$Ef = 0.056 + 0.54\ \frac{t}{l_e} \tag{68}$$

Resulting failure strain obtained for LS-DYNA mesh element size is equal to 0.24 and 0.31 for ANSYS. It is worth noting that to activate element deletion in ANSYS, it is necessary to program in each of the cycles a total model check for each one of the sub-steps.

3.9.1. Case: mild steel stiffened plate

The following graphs show, for different shock factors bearable by the mild steel structure without reaching rupture strain, a comparison of the maximum deflection obtained with LS-DYNA and ANSYS. It is worth to clarify that for this set of tests, the beam sections are slightly different in each of the models. Indeed, for the case of the beam used in ANSYS is the HP180X8, and the beam used in LS-DYNA is simplified as a rectangular section beam with about the same dimensions.

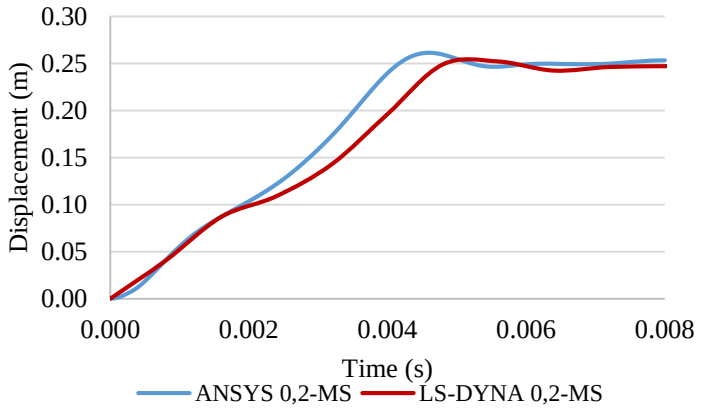

Figure 49. Mild steel central nodal displacement for a shock factor of 0.2.

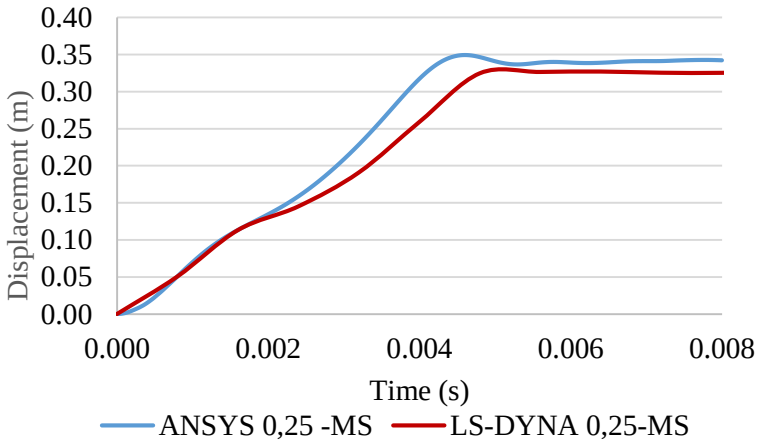

Figure 50. Mild steel central nodal displacement for a shock factor of 0.25.

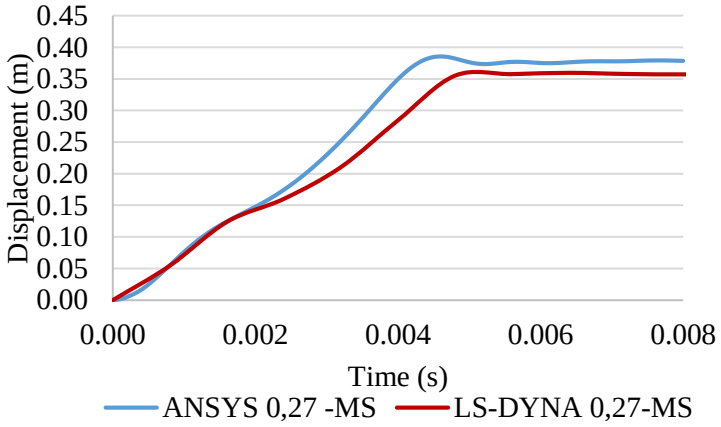

Figure 51. Mild steel central nodal displacement for a shock factor of 0.27.

It can also be seen from Table 8 below that the discrepancy between LS-DYNA and ANSYS obtained deflections does not exceed 6.2 % for the case of the mild steel.

Table 8. Deflections comparison for mild steel.

SF	LS-DYNA	ANSYS	ERROR %
0,2	0,25	0,25	2,89
0,25	0,33	0,34	5,35
0,27	0,36	0,38	6,16

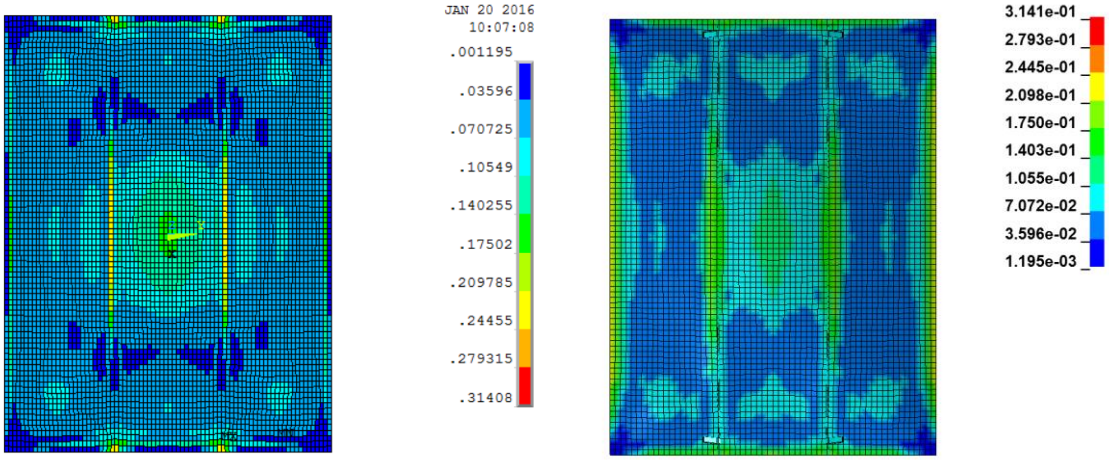

Figure 52: Mild steel - Equivalent plastic strain for shock factor: 0.27
ANSYS (Left) - LS-DYNA (RIGHT).

3.9.2. Case: quench steel stiffened plate

When the plate and its stiffeners are constituted by quench steel, maximum deflections obtained with ANSYS and LS-DYNA are also similar, as shown in figures 53, 54 and 55. These figures show also the capacity of the quench steel to withstand a bigger shock factor without presenting rupture.

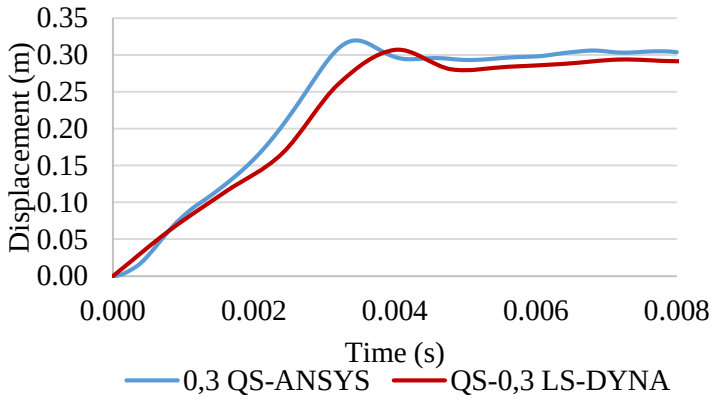

Figure 53. Quench steel central nodal displacement for a shock factor of 0.3.

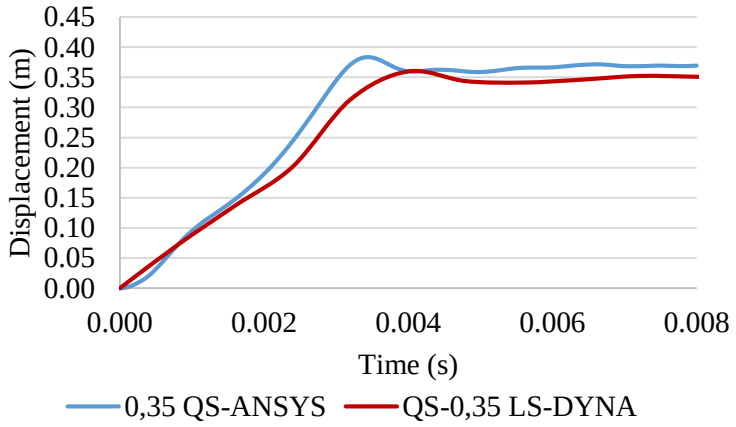

Figure 54. Quench steel central nodal displacement for a shock factor of 0.35.

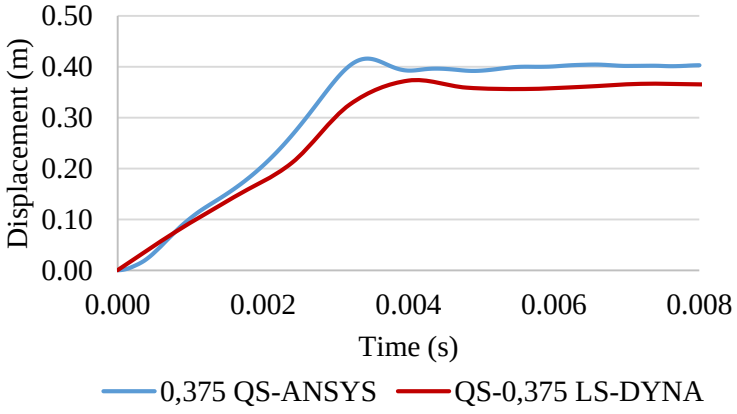

Figure 55 Quench steel central nodal displacement for a shock factor of 0.375.

The discrepancies between LS-DYNA and ANSYS results can be seen in the following table.

Table 9. Deflections comparison for quench steel.

SF	LS-DYNA	ANSYS	ERROR %
0,3	2,94	3,04	3,40
0,35	0,35	0,36	4,82
0,375	0,36	0,40	9,86

The repartitions of effective plastic strain are depicted in Figure 56 for the biggest shock factor. The differences in the pattern of the strain for this case, is due to the fact that the simulation done in ANSYS reaches a larger deformation. Although the maximum effective plastic strain values are sensitively different at the end of the load step, the rupture strain found for both simulations has been barely reached.

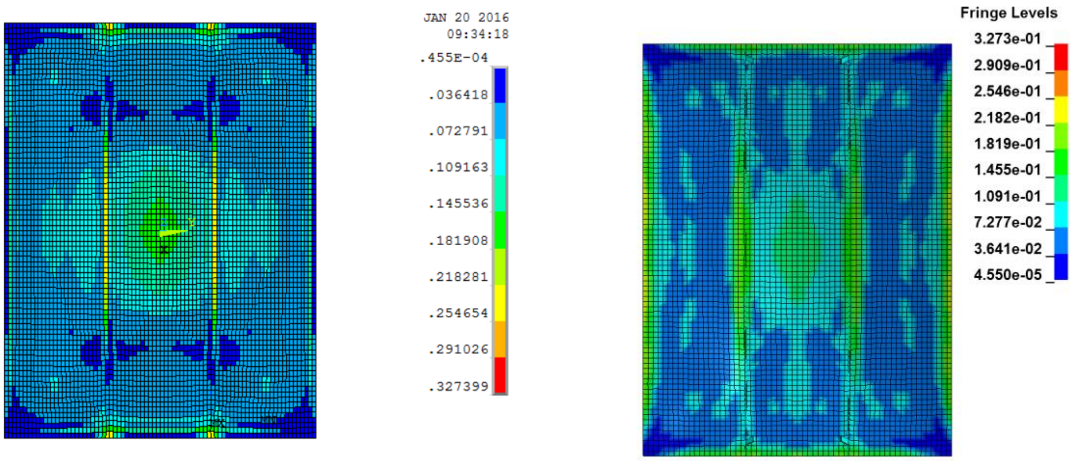

Figure 56: Quench steel - Equivalent plastic strain for shock factor 0.375
ANSYS (Left) - LS-DYNA (RIGHT)

Comparison between ANSYS and LS-DYNA results were also performed for bigger shock factors but without simulating the plate failure, i.e. without activating the erosive law.

As shown in Figure 6, obtained maximum deflections can be very different. This is due to the fact that very large (and nonphysical) plastic deformations are not handled the same way by the implicit solver of ANSYS and the explicit solver of LS-DYNA. This also means that results between the 2 codes are only comparable up to the rupture of the plate, which must be simulated using for example an erosive law.

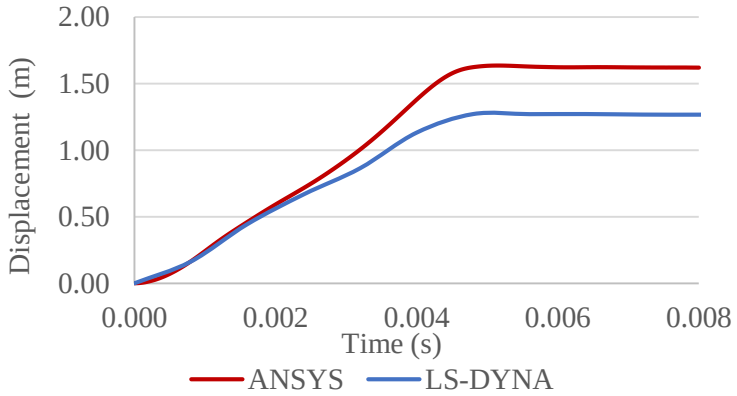

Figure 57: (Non-physical) deflection of the stiffened plate center for the shock factor of 0.841 without taking into account the erosive law.

3.10. Ship-section UNDEX analysis

The general dimensions used for the ship section scantling can be seen in Figure 58. The top plate of the scantling which is not displayed has a thickness of 11 mm. The section of the stiffeners was originally made in ANSYS using two HP180X8 for the smaller section and three HP160X7 for the bigger section, and using rectangular stiffeners in LS-DYNA. The results of this work can be seen at the appendices A2. To avoid incongruences, a set of simulations were made using the rectangular BEAM188 stiffeners in ANSYS and BEAM elements in LS-DYNA, the objective being to have exactly the same finite element model, and also the same meshing.

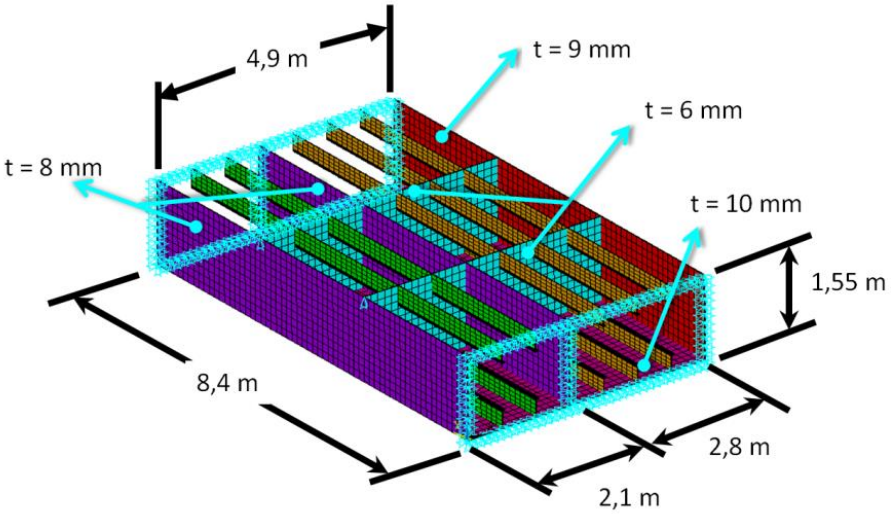

Figure 58. General dimensions of the scantling

Figure 59 shows the finite element model of the ship section proposed by STX as well as the principal dimensions and considered boundary conditions.

For both ANSYS and LS-DYNA models, the failure strain thresholds value is calculated using the Lehmann's formula and is equal to 0.09457 (the average length of shell finite elements is around 14 cm and the bottom thickness is 10 cm).

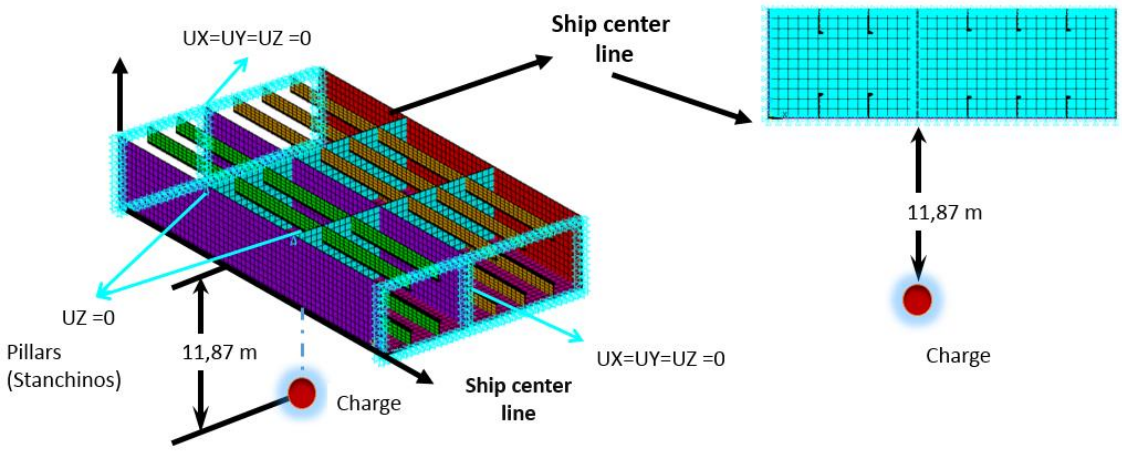

Figure 59. Ship section scantling used.

Numerical simulations were performed both for materials quenched steel and mild steel, following the same approach as for the stiffened plate. The shock factor was thus progressively increased up to the failure of one finite element. Figure 60 shows, for shock factors 0.378 and 0.488, the time evolution of the shock wave pressure which is applied to the structure,.

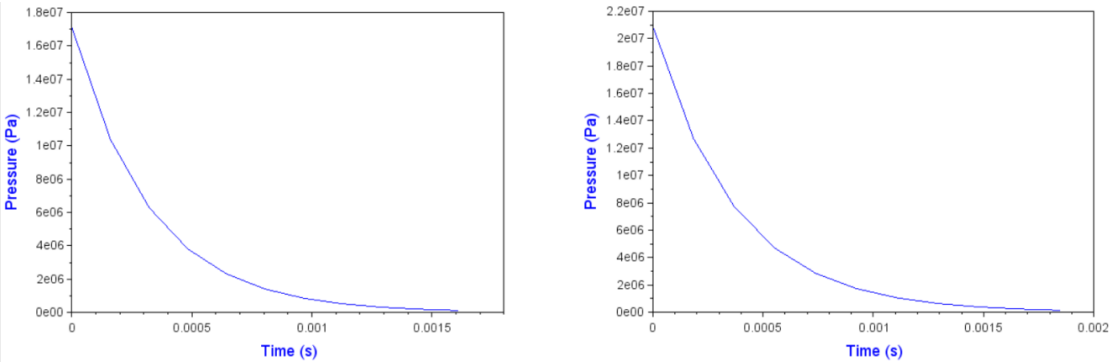

Figure 60. Time history pressure applied to the struture. SF 0.378 (left) and SF 0.488 (right).

The following graph also shows the pressure distribution for the first step in ANSYS onto the structure. The color pattern verifies that the spherical wave approximation is being used, by the pressure distribution observed at the bottom of the plate.

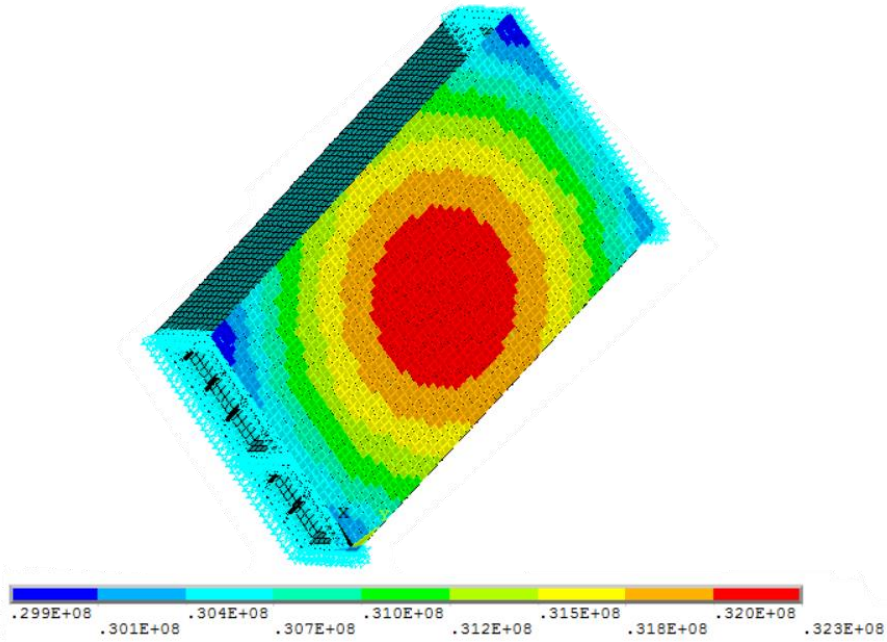

Figure 61. Initial step pressure input applied to the structure using the spherical wave approximation. Pressure applied in Pa.

Figure 62 shows the location of the nodes which deflection time history has been post-processed, both in LS-DYNA and ANSYS.

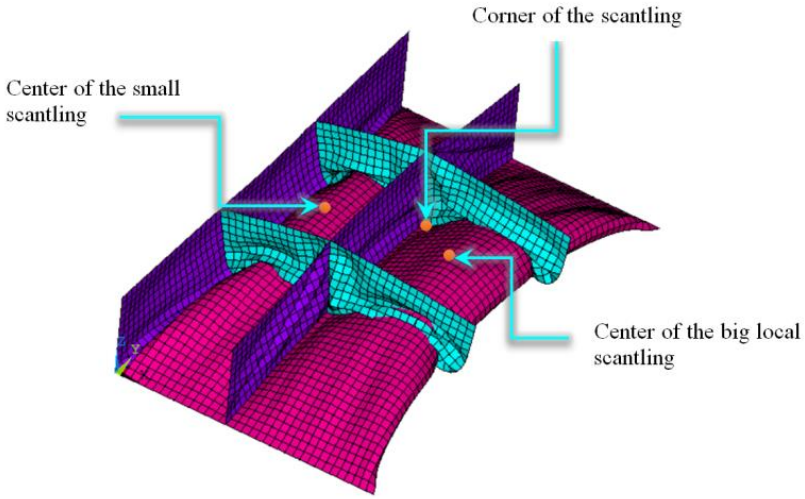

Figure 62. Points measured on the structure.

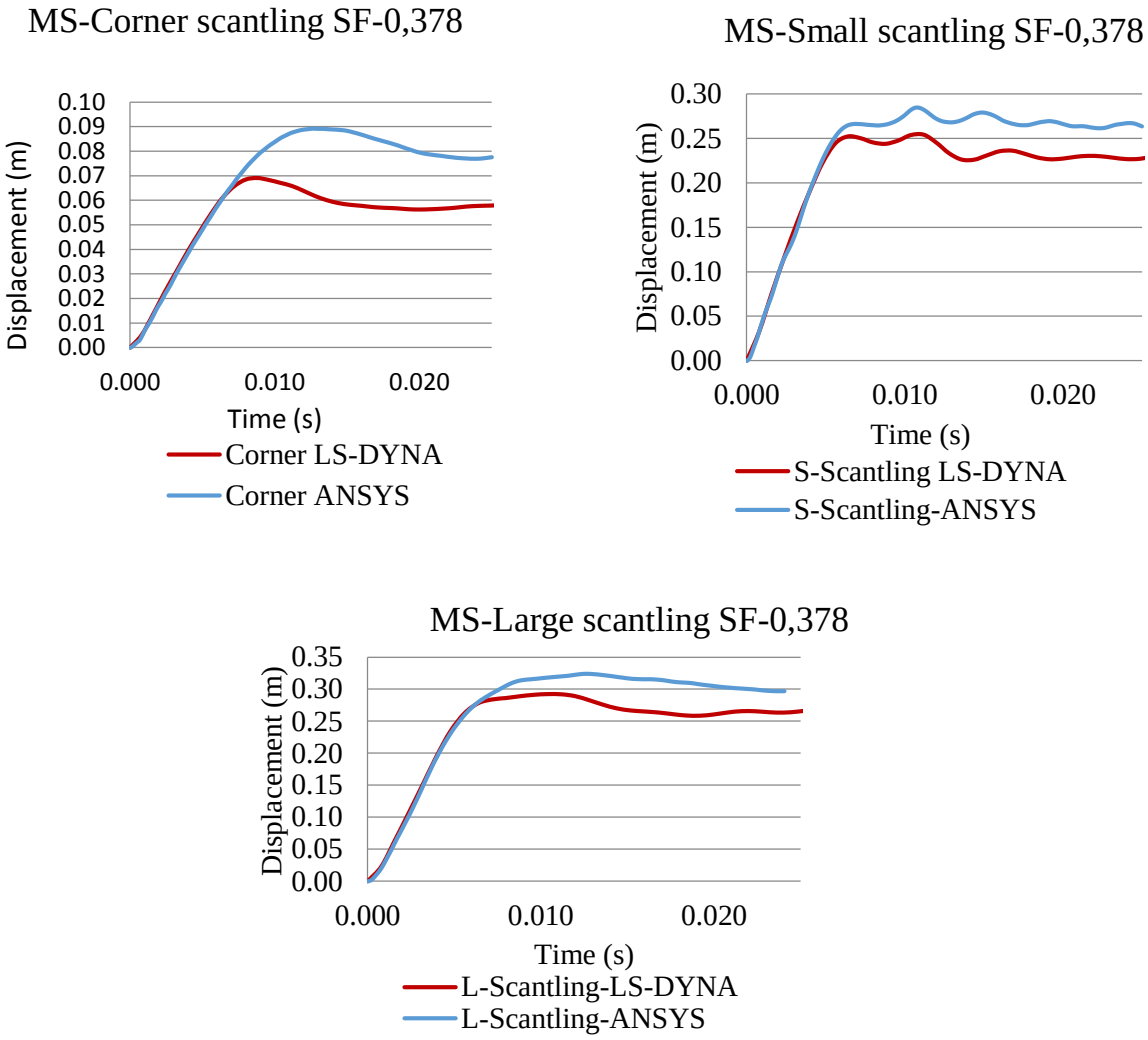

Figure 63 Mild steel. – Deflection at 3 different locations.

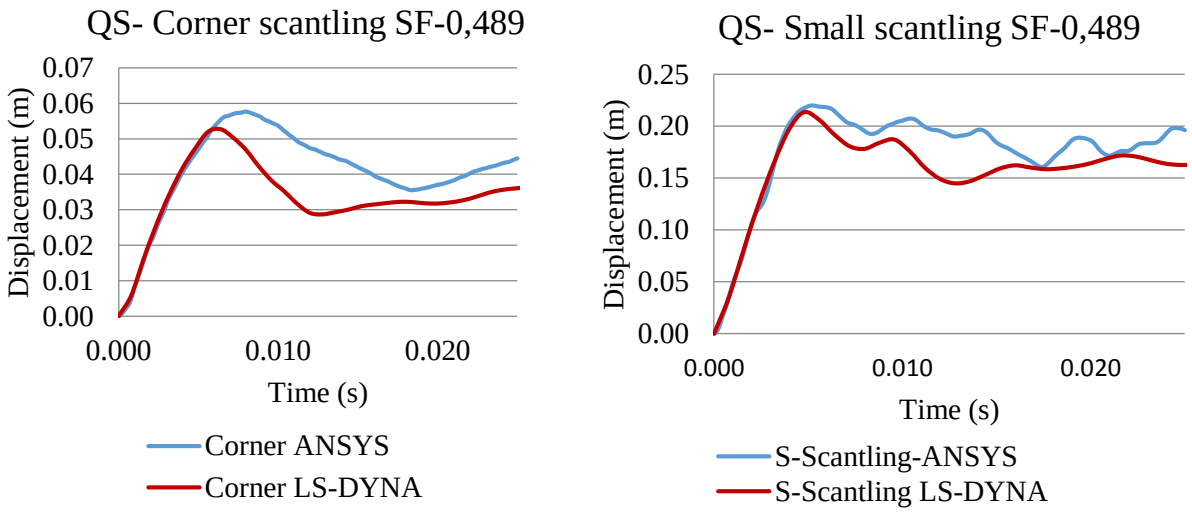

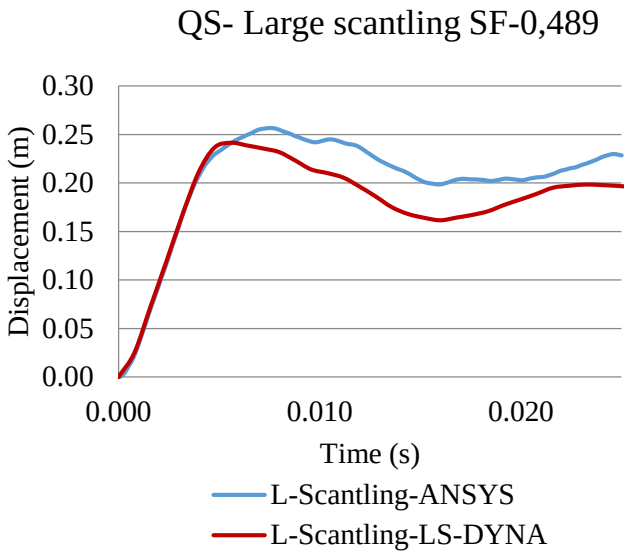

Figure 64: Quench steel. – Deflection at 3 different locations

As it can be seen on these figures, although some noticeable differences appear during the elastic release phase, the final plastic deflections of the plate at the post-processed nodes are globally in good accordance. Figures 65 and 66 present the repartition of the effective plastic strain at the end of the simulation, respectively for the mild steel section and for the quench steel one. Whatever is the steel material, it is observed that the plastic strain patterns are very similar between ANSYS and LS-DYNA.

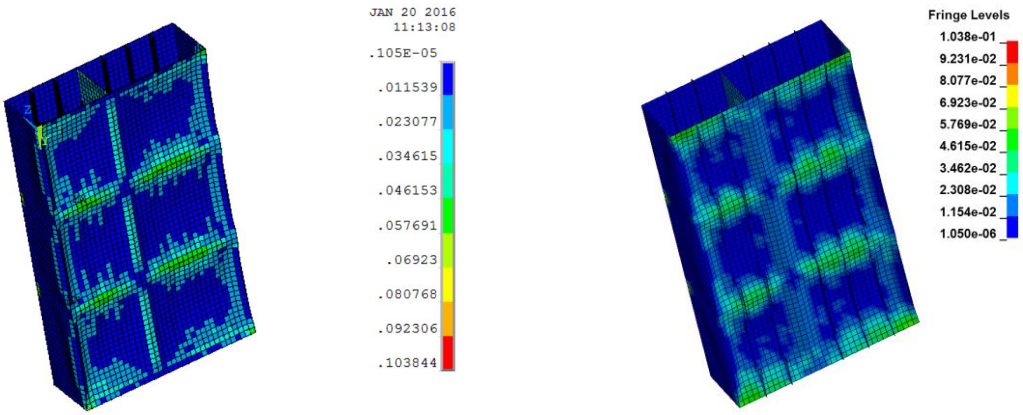

Figure 65. Mild Steel-Repartition of effective plastic Strain SF:0.31
ANSYS (LEFT) - LS-DYNA (RIGHT).

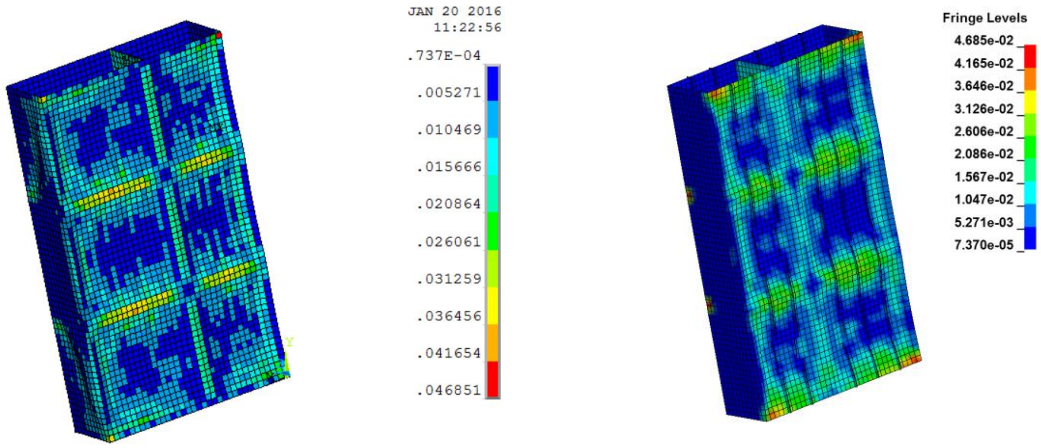

Figure 66.Quench Steel- Repartition of effective plastic Strain. SF:0.33.
ANSYS (LEFT) - LS-DYNA (RIGHT).

4. CONCLUSIONS

- A general review on the disclosed rules has been made, focusing on the procedure that can be performed by the tools available at STX Europe, such as the finite element tool ANSYS.

- The work was particularly focused on the analysis of plates, stiffened plates and finally a ship section subjected to a non-contact underwater explosion. For the work initially performed using the experimental data form single plates subjected to underwater explosions.

- The initial velocity formulation did not meet the requirements by underestimating the value of final deformation that the plate will have. On the other hand the use of the pressure history applied to the plate showed better results, motivating the continuation on the study in the regular stiffened panel and the simplified ship section for further review.

- It was proven that the numerical simulations using LS-DYNA and ANSYS end up having approximately similar results for all of the models here proposed. The results must not be trustable when the rupture of the plate is reached. In other words the results must be as physical as possible in order to have accordance.

- Comparing the results obtained using the LS-DYNA explicit solver with the results obtained using the ANSYS implicit one, it is shown that slight discrepancies may occur. Those discrepancies are probably due to the solvers themselves and to the formulation of the shell elements. It also is worth noting that an implicit solver like ANSYS is more adequate for nonlinear quasi-static problems, while an explicit solver like LS-DYNA is preferably used to simulate fast dynamic problems.

5. ACKNOWLEDGEMENTS

I would to express my gratitude to all the people that contributed in the development of this work, especially to the Professor Doctor Hervé Le Sourne, who carefully followed my work, without forgetting all of the wonderful people I met at ICAM including professors and students. Also to the company STX Europe where I had the chance to perform my internship, and particularly to the department of Acoustic and Vibrations lead by the Engineer Sylvain Branchereau and also specially to the Engineer Lucas Clement who did not hesitate to collaborate on my work. Additionally I would like to express my appreciation to the Lloyd's Register Foundation which has provided the financial support in the development of my studies at the EMHIP program.

Finally I would like to give the recognition to my family who have always supported me with love in all of the projects I pose in my life.

This thesis was developed in the frame of the European Master Course in "Integrated Advanced Ship Design" named "EMSHIP" for "European Education in Advanced Ship Design", Ref.: 159652-1-2009-1-BE-ERA MUNDUS-EMMC.

6. REFERENCES

Gupta, N., Kumar, P., & Hegde, S. (2010). On deformation and tearing of stiffened and un-stiffened square plates subjected to underwater explosion—a numerical study. *International Journal of Mechanical Sciences*, 733-744.

(BV), G. N. (1973). *Construction Specifications for Bundeswehr Vessels.*

Alexander, J. E. (2009). Shock Response Spectrum – A Primer. *Sound and Vibration Magazine*, 6-14.

Barras, G. (2007). *Réponse dynamique des structures aux explosions sous-marines.* These de Máster SMA, École Centrale de Nantes.

Chul-Hong, K., & Young S., S. (2012). Numerical simulation of surface shield effects to waterblast wave. *Ocean Engineerign*, 99-114.

Clements, E. (1972). *Shipboard Shock And Navy Devices for its Simulation.* Washington D.C.: Naval Ressearch Laboratory.

Cole, R. (1946). *Underwater explosions.* Princeton: Princeton University Press.

DeRuntz Jr, J. J. (1994). *The Underwater Shock Analysis Code And Its Applications.* Lockheed Palo Alto Research Laboratory, Computational Mechanics Laboratory, Palo Alto.

Didoszak, L. J., Shin, D. Y., & Lewis, C. D. (2001). *Shock Trial Simulation for Naval Ships.* Livermore, CA: XYZ Scientific Applications, Inc., TrueGrid User's.

Ding, P., & Buik, A. (2015, 07 03). *MSCSOFTWARE*. Retrieved from Simulation of Under Water Explosion using MSC.Dytran : http://www.mscsoftware.com/assets/3032_Under_Water_Explosion_SAVIAC.pdf

Edgerton (Director). (1943). *Underwater Explosion Phenomena* [Motion Picture].

Elsaye, F., Hui, Q., Lili, T., & Mahmoud, H. (2014). Numerical Simulation and Response of Stiffened Plates Subjected to Noncontact Underwater Explosion. *Advances in Materials Science and Engineering*.

Elsayed, F., Hui, Q., Lili, T., & Helal, M. (2014). Numerical investigation of the dynamic response of optimized composite elliptical submersible pressure hull subjected to non-contact underwater explosion. *Composite Structures*, 121-133.

Emre Demír, M. (2015). *Shock analisys of an antenna structure subjected to underwater explsoins.* Middle East Technical University.

Feng, X., Yong, C., Yu, W., Hongxing, H., & Dawei, Z. (2014). Experimental Research on the Dynamic Response of Floating Structures with Coatings Subjected to Underwater Explosion. *Shock and Vibration*.

Hollyer, R. S. (1959). *Direct Shock-Wave Damage to Merchant Ships From Non Contact Underwater Explosions.* Norfolk Naval Shipyard.

Hsu, C.-Y., Liang, C.-C., Nguyen, A.-T., & Teng, T.-L. (2013). A numerical study on the underwater explosion bubble pulsation. *Ocean Engineering*, 29-38.

ISSC. (2006). 16th INTERNATIONAL SHIP AND OFFSHORE STRUCTURES CONGRESS., *1*, pp. 35-38. Southhampton, UK.

J. O'Hara, G., & O. Belsheim, R. (1963). *Interim Desing alues for shock desing of shipboard equipment* . Naval Research Laboratory., Department of the Navy, Washington D.C.

Keil, A. (1961). *The response of ships to underwater explsions.* (S. o. Engineers, Ed.) New York, Armed Services Technical information Agency, United States Of América.

Liang, C.-C., & Tai, Y.-S. (2006). Shock responses of a surface ship subjected to noncontact underwater explosions. *Ocean Engineering*, 748-772.

Liang, Cho-Chung; Yang, Min-Fang; Tai, Yuh-Shiou. (2002). Prediction of shock response for a quadropod-mast usinng the response spectrum analysis method. *Ocean Engineering*, 887-914.

Mair, H. U., & M. Reeve, R. (1998). *Simulated Ship Shock Test/Trials?* Kurt Hartsough Surface Warfare Center, Carderock Division, Naval Business Center, Philadelphia.

McCarthy Jr., R. H. (1995). *Shock Design Criteria For Surface Ships.* NAVSEA, Ship Survivality and Structural Integrity Group. Direction of commander, Naval Sea Systems Command.

Mehaute, B. L., & Wang, G. (1996). *Water Waves Generated By Underwater Explosions.* Miami.

Miller, S., Jasak, H., Boger, D., Paterson, E., & Nedungadi, A. (2012). A pressure-based, compressible, two-phase flow finite volume method. *Computers & Fluids*, 1-11.

NAVY, U. (2015, 12 05). *Al-Bab*. Retrieved from www.al-bab.com/yemen/cole1.htm

NRL. (1965). *Background for Mechanical Shock Design Of Ships Systems.* Springfield.

Nu, Z., Zhi, Z., & Wepeng, Z. (2014). Dynamic response of a surface ship structure subjected to an underwater explosion bubble. *Marine Structures*, 26-44.

O'Daniel, J., Krauthammer, T., Koudel, K. L., & Strait, L. H. (2002). An UNDEX response validation methodology. *International Journal of Impact Engineering*, 919-937.

Plesset, & Prosperetti. (1977). Bubble dynamics and cavitation. *Annual Review of Fluid Mechanics*, 145-185.

Prior, M. K., & Brown, D. J. (2010). Estimation of Depth and Yield of Underwater Explosions From First and Second Bubble-Oscillation Periods. *IEEE JOURNAL OF OCEANIC ENGINEERING*, 103-112.

Ramajeyathilagam, K., & Vendhan, C. (2004). Deformation and rupture of thin rectangular plates subjected to underwater shock. *International Journal of Impact Engineering*, 699-719.

Ramajeyathilagam, K.; Vendhan, C.P.; Bhujanga Rao, V. (2000). Non-linear transient dynamic response of rectangular plates under shock loading. *International Journal of Impact Engineering*, 999-1015.

Rayleig, L. (1917). On the Pressure developed in a Liquid during the Collapse of a Spherical Cavity. *Philosophical Magazine*.

Reid, W. D. (1996). *The Response of Surface Ships to Underwater Explosions.* Department of Defence, Ship Structures and Materials Division Aeronautical And Maritime Laboratory, Melbourne Victoria.

Simoens, B., & H. Lefebvre, M. (2011). Influence of Different Parameters on the TNT-Equivalent. *Central European Journal of Energetic Materials*, 53-67.

Tao, J. (2009). The Analysis on shock design spectrum of shipboard. *Intelligent Computing and Intelligent Systems*, 748-751.

Vernon, T. A. (1986). *WHIPPING RESPONSE OF SHIP HULLS FROM UNDERWATER EXPLOSION BUBBLE LOADING.* Defense Research Establishment Atlantic, Dartmouth.

Wang, H., Wang, Y., & Chen, G. (2008). Time Domain Analysis of Shock Response of Pipeline on Ship. *IMAC-XXVI: Conference & Exposition on Structural Dynamics - Technologies for Civil Structures.* Society for experimental mechanics (SEM).

Xiong-liang, Y., Qi-xin, Z., A-man, Z., & FENG, L.-h. (2008). Numerical simulation of the anti-shock performance. (Springer, Ed.) *Journal of Marine Science and Application*, 33-39.

Zong, Z., Zhao, Y., & Li, H. (2013). A numerical study of whole ship structural damage resulting from close-in underwater explosion shock. *Marine Structures*, 24-43.

7. APPENDICES

A1. Results summary from the experiemtal results obtained from (Ramajeyathilagam, K.; Vendhan, C.P.; Bhujanga Rao, V., 2000), and the results obtained usign ANSYS and LS-DYNA.

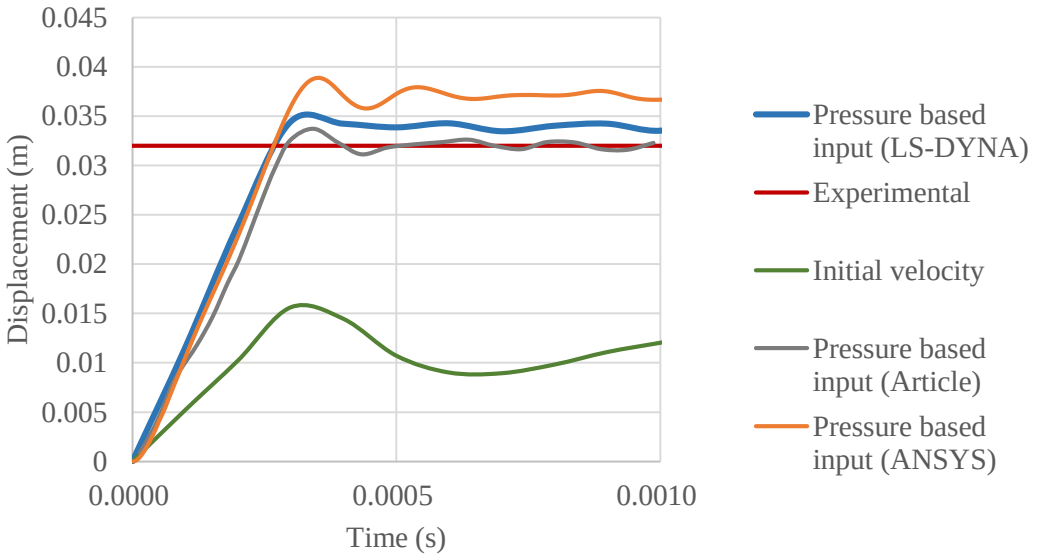

Figure 67. High stregth steel shock factor: 0.424.

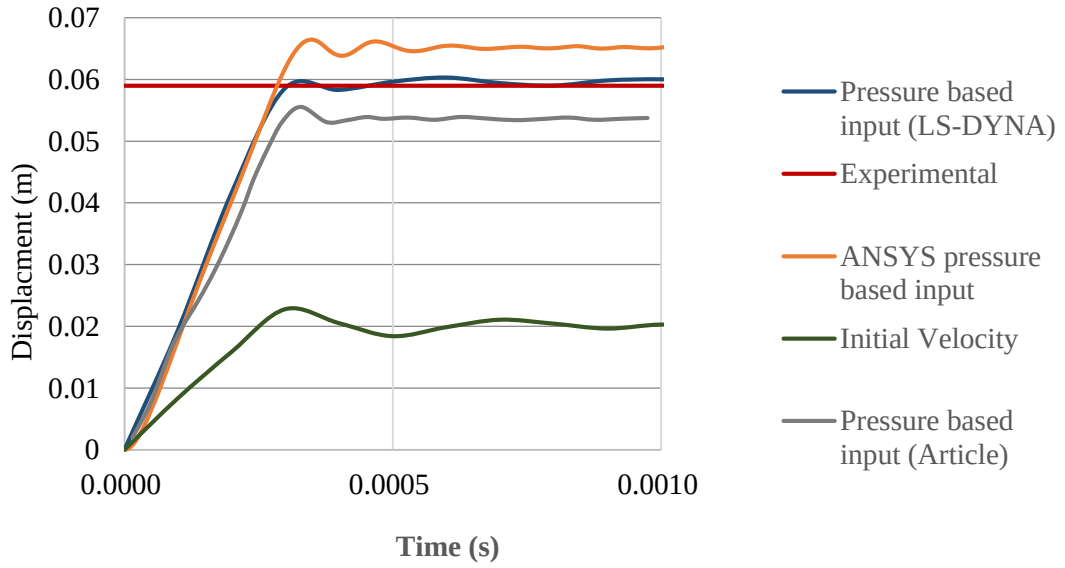

Figure 68. High stregth steel shock factor: 0.671.

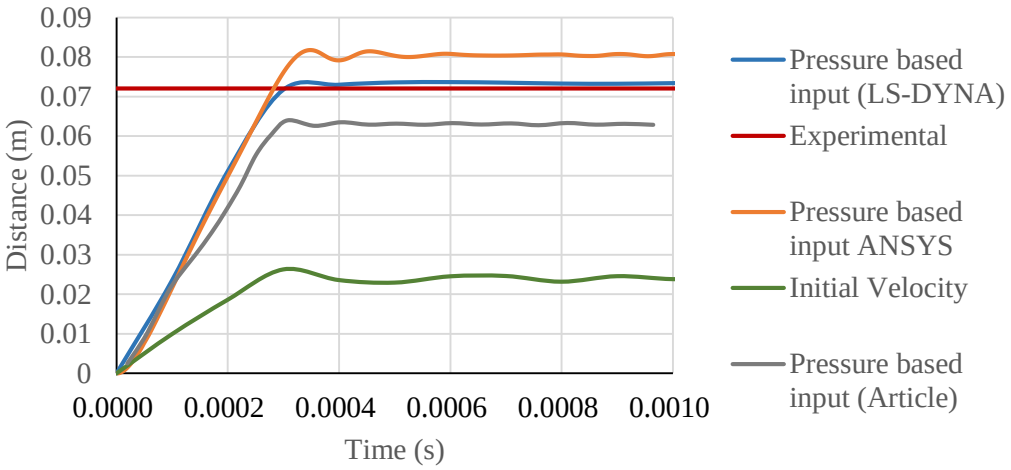

Figure 69. High strength steel shock factor: 0.794

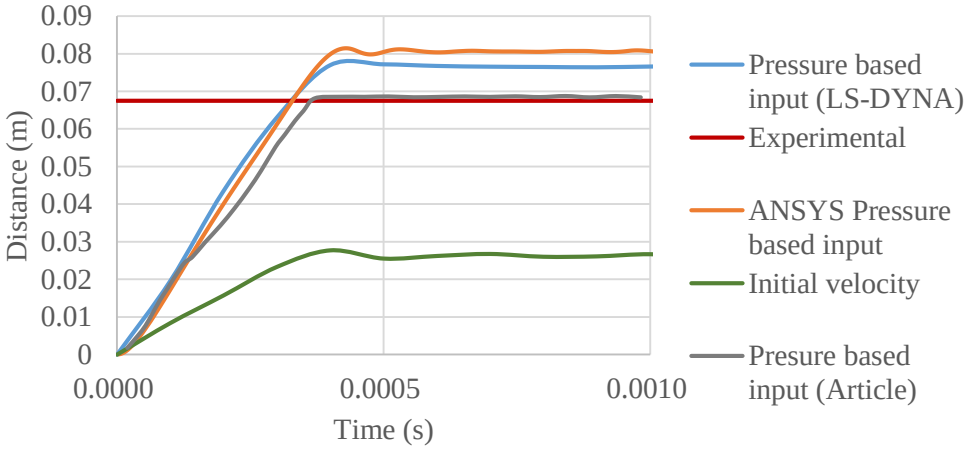

Figure 70. Mild steel shock factor: 0.671.

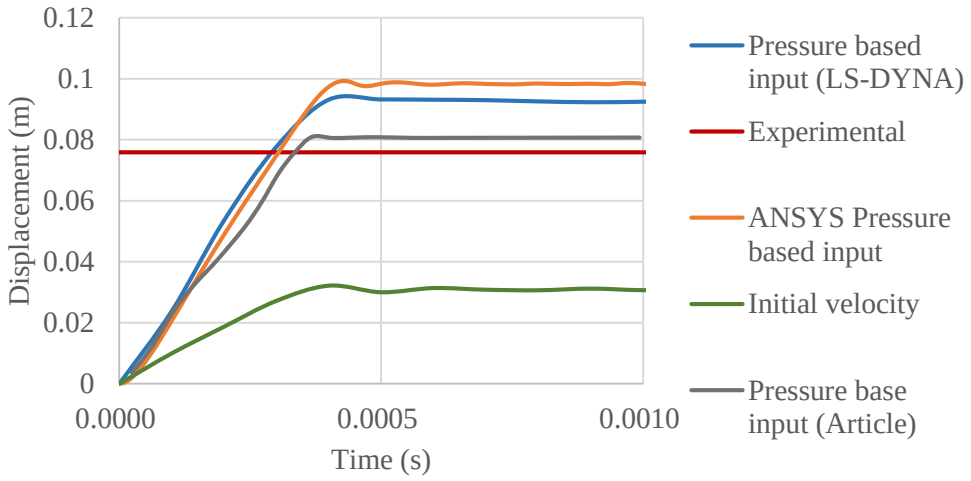

Figure 71. Mild steel shock factor: 0.794.

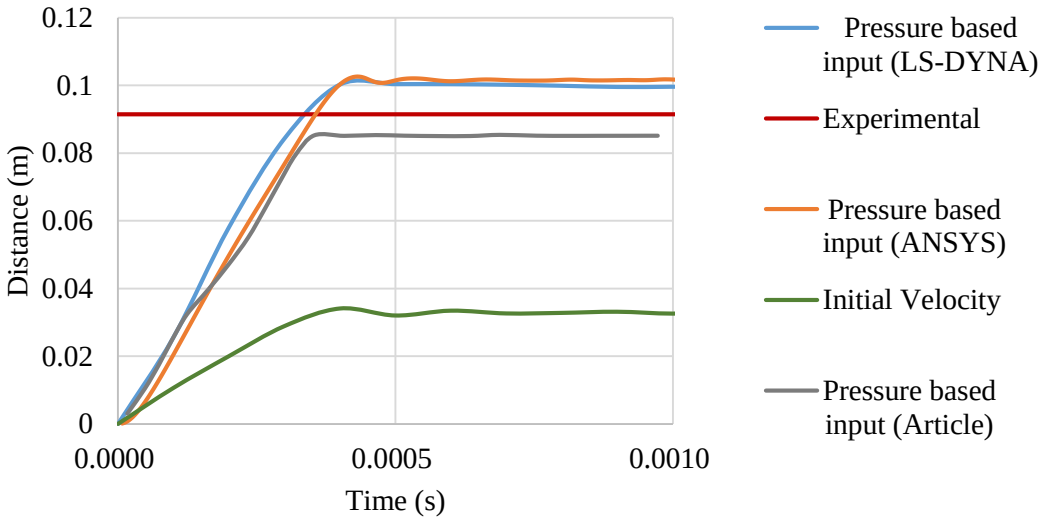

Figure 72. Mild steel shock factor: 0.894.

A2. Displacement time history points of a ship section comparison using LS-DYNA and ANSYS for Quench Steel and Mild Steel, using HP stiffeners in ANSYS and rectangular equivalent sections in LS-DYNA.

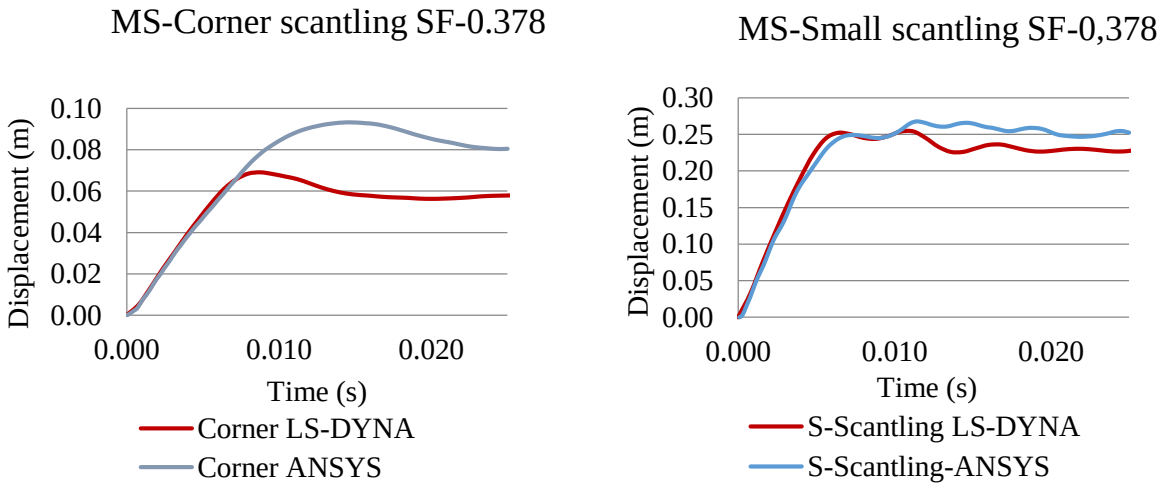

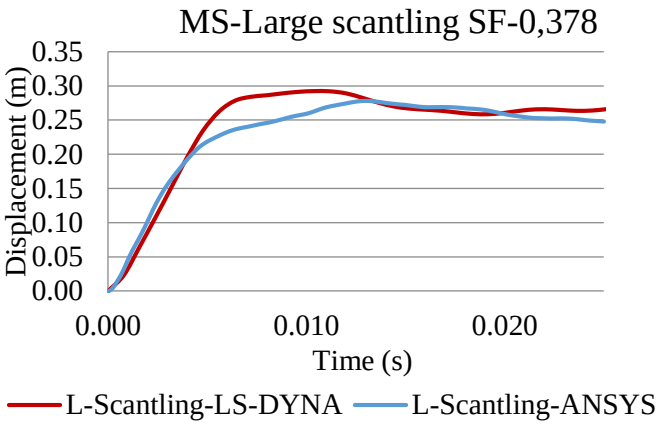

Figure 73. Measurement of deflections at three different locations for the scantling using Mild steel.

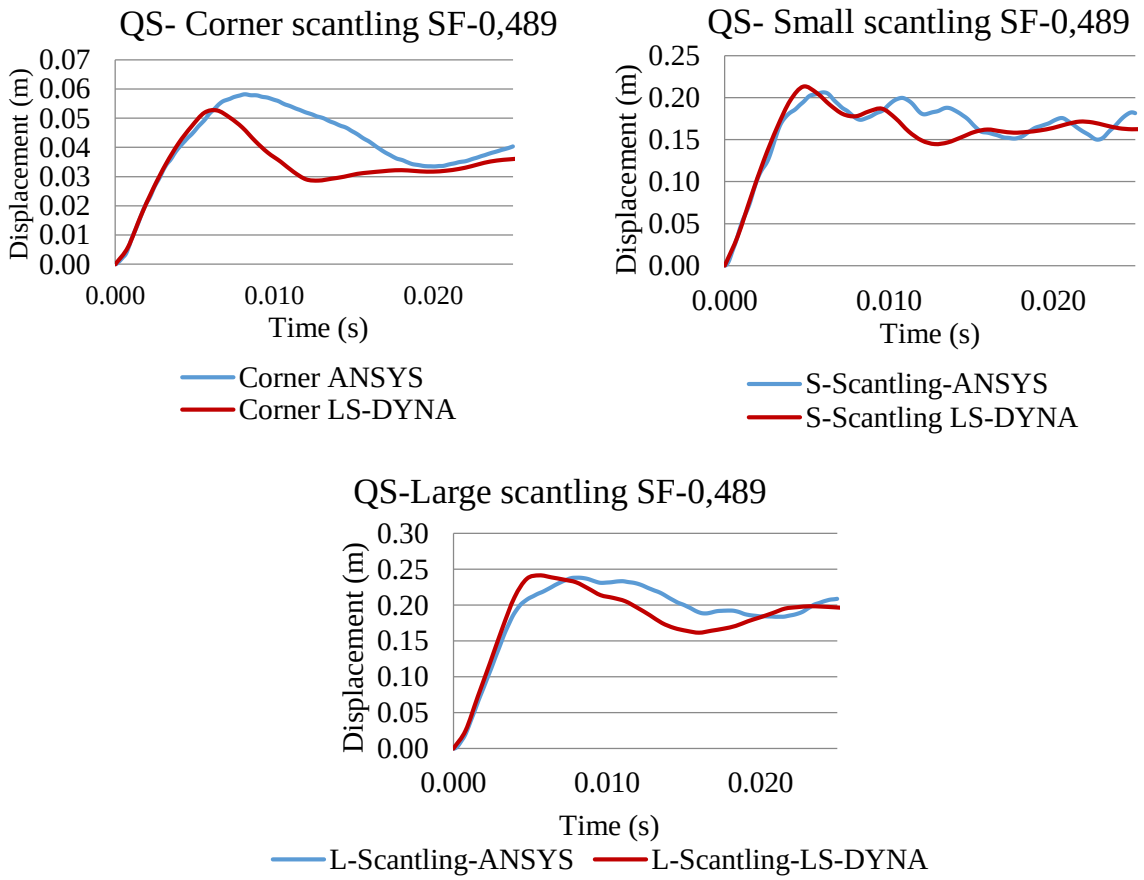

Figure 74. Measurement of deflections at three different locations for the scantling using Quench steel.